

The spread of awareness and its impact on epidemic outbreaks

Sebastian Funk^{a,1}, Erez Gilad^a, Chris Watkins^b, and Vincent A. A. Jansen^a

^aSchool of Biological Sciences and ^bDepartment of Computer Science, Royal Holloway, University of London, Egham TW20 0EX, United Kingdom

Edited by Bryan Grenfell, Penn State University, Erie, PA, and accepted by the Editorial Board February 11, 2009 (received for review October 27, 2008)

When a disease breaks out in a human population, changes in behavior in response to the outbreak can alter the progression of the infectious agent. In particular, people aware of a disease in their proximity can take measures to reduce their susceptibility. Even if no centralized information is provided about the presence of a disease, such awareness can arise through first-hand observation and word of mouth. To understand the effects this can have on the spread of a disease, we formulate and analyze a mathematical model for the spread of awareness in a host population, and then link this to an epidemiological model by having more informed hosts reduce their susceptibility. We find that, in a well-mixed population, this can result in a lower size of the outbreak, but does not affect the epidemic threshold. If, however, the behavioral response is treated as a local effect arising in the proximity of an outbreak, it can completely stop a disease from spreading, although only if the infection rate is below a threshold. We show that the impact of locally spreading awareness is amplified if the social network of potential infection events and the network over which individuals communicate overlap, especially so if the networks have a high level of clustering. These findings suggest that care needs to be taken both in the interpretation of disease parameters, as well as in the prediction of the fate of future outbreaks.

mathematical model | rumor spread | behavioral response | social networks

Human reactions to the presence of disease abound, yet they have rarely been systematically investigated (1). Such reactions can range from avoiding social contact with infected individuals (*social distancing*) to wearing protective masks, vaccination, or more creative precautions. It has been shown, for instance, that local measles outbreaks are correlated with the demand for measles, mumps, and rubella vaccines (2). Similarly, the demand for condoms rises in areas where AIDS is prevalent (3), and condom use has been linked to the knowledge of someone who has died of AIDS (4).

Behavior that is responsive to the presence of a disease can potentially reduce the size of an epidemic outbreak. On closer inspection, it is not so much the presence of the disease itself that will prompt humans to change their behavior, as *awareness* of the presence of the disease. A change in behavior can be prompted without witnessing the disease first hand, but by being informed about it through others. This information in itself will spread through the population and have its own dynamic. For example, according to the Chinese Southern Weekend newspaper, the text message “There is a fatal flu in Guangzhou” was sent 126 million times in Guangzhou alone during the 2003 severe acute respiratory syndrome (SARS) outbreak (5), causing people to stay home or wear face masks when going outside. This figure stands in stark contrast to the comparatively low number of 5,327 cases recorded in the whole of China (6). It is not clear how much the individual behavioral responses contributed to containing the disease.

The spread of rumors has been described as “infection of the mind” (7) or “thought contagion” (8), and their spread is analogous to the spread of an infectious disease: information is passed on from carrier to carrier through a network of contacts. Therefore, when humans respond to the presence of a disease, we have a situation where an infectious agent and the information about

the presence of this agent spread simultaneously, and will interact in their spread by a change in human behavior.

Here, we present a network model for the spread of awareness about a contagious disease. Awareness arises at the location of the disease and spreads among the population similarly to the way a disease would, an analogy that was suggested as early as 1964 (9). To capture the ephemeral nature of information, we implement an idea presented in ref. 10: as the information is passed from person to person, it loses its *quality*; in other words, first-hand information about a disease case will lead to a much more determined reaction than information that has passed through many people before arriving at a given individual.

Efforts to assess the potential for prevention of future outbreaks of contagious diseases have motivated previous studies on the effects of social distancing (11, 12) which, however, focused on behavioral changes imposed by a central organization on the population level. Attempts at extending this to incorporate individual behavioral reactions have focused on vaccination decisions and consequences thereof (13–16), dynamic rewiring of transmissive contacts (17), or incidence-dependent reductions in contact rate (18).

In this study, we will investigate how the spread of awareness, prompted by first-hand contact with the disease, affects the spread of a disease. In this context, we understand awareness as the possession of information about the outbreak one is willing to act on as opposed to just generally knowing about the disease through media coverage or government programs without taking action. To study this, we have overlaid our model of information spread with a model for the spread of a contagious disease on two, not necessarily identical networks, with more informed individuals acting to reduce their susceptibility.

In the following, we will introduce the model and, in a first approximation, cast it into a system of ordinary differential equations under the assumption of random mixing of individuals within the population. This will allow us to show how awareness can reduce the number of individuals infected during an epidemic, while the threshold for disease invasion, and thus the potential for outbreaks, remains unchanged. Subsequently, we will consider a full spatial version of the same model. We will see that if the assumption of random mixing is lifted and the local nature of the interaction taken into account, locally spreading awareness can prevent a disease from breaking out, and how social network structure and overlap between the networks have an effect on this interaction.

The Model

We associate with each individual X in the population of size N a level of awareness indicated by an index i which denotes the

Author contributions: S.F., E.G., C.W., and V.A.A.J. designed research; S.F., E.G., and V.A.A.J. performed research; S.F. analyzed data; and S.F. and V.A.A.J. wrote the paper.

The authors declare no conflict of interest.

This article is a PNAS Direct Submission. B.G. is a guest editor invited by the Editorial Board.

¹To whom correspondence should be addressed. E-mail: s.funk@rhul.ac.uk.

This article contains supporting information online at www.pnas.org/cgi/content/full/0810762106/DCSupplemental.

Table 1. Transitions of the model

	Transition	Rate
Infection	$S_i + I_j \rightarrow I_i + I_j$	$(1 - \rho^i)\hat{\beta}$
Recovery	$I_i \rightarrow R_i$	γ
Information transmission	$X_i + X_{j>(i+1)} \rightarrow X_i + X_{i+1}$	$\hat{\alpha}$
Information fading	$X_i \rightarrow X_{i+1}$	λ
Information generation	$I_i \rightarrow I_0$	ω

number of passages the information has undergone before arriving at the given individual, i.e., X_0 will stand for an individual with first-hand information and X_i for one with information that has passed through i other individuals before arriving at the given individual. The two transitions governing the information dynamics are *information transmission* ($X_i + X_{j>(i+1)} \rightarrow X_i + X_{i+1}$) and *fading of awareness* ($X_i \rightarrow X_{i+1}$). As the quality of information decreases at each transmission event while it is also gradually lost within each individual, information eventually disappears from the population if it is not refreshed.

We link this model to an epidemiological susceptible-infected-recovered (SIR) model (19), assigning each individual a disease-related state of susceptible (denoted S_i , the subscript i again representing the level of information), infected (I_i) or recovered (R_i) with the usual transitions of *infection* and *recovery*.

To capture the impact of individual actions, we make transmission of the disease dependent on the quality of the information available to a given susceptibility. The susceptibility of individuals in states S_i increases with i as $(1 - \rho^i)$, $0 < \rho < 1$. The decay constant ρ therefore governs how much the tendency to act is reduced with decreasing quality of information. The total amount of awareness in the susceptible part of the population $g(\rho, \{S_i(t)\})$ at any given time t can then be calculated as $g(\rho, \{S_i(t)\}) = \sum (S_i(t)/S(t))\rho^i$, $i = 0, 1, 2, \dots$, the probability generating function of awareness within susceptibles.

We assume that information can be generated de novo if the disease is present, so we link generation of new information to a transition through which awareness about the disease is generated in infected individuals at rate ω . As the parameter ω thus reflects the likelihood per unit time of an infected individual to find out about their infection, it distinguishes between diseases with obvious and readily interpreted symptoms and cases where, for instance, the infection is contagious but asymptomatic, or where infection does not necessarily entail awareness about its nature (e.g., SARS, which may be mistaken for common flu). All the transitions and their respective rates are summarized in Table 1. There, and in the following, we denote with a hat per contact as opposed to population-level rates such that $\hat{\alpha}$ is the rate of information transmission per contact, whereas α is the total rate of information in the population, and analogously for β and $\hat{\beta}$. This is relevant only for the contact processes governed by these two parameters, because the processes not depending on contact happen with the same rate at the individual level as at the population level.

Mean-Field Analysis

In the mean-field approximation, individual variables are replaced by population aggregates. By assuming random mixing and therefore ignoring any spatial structure within the population, we can describe the model system fully considering only the number of individuals in each possible state.

In the mean-field version of our model of information spread, the population is compartmentalized according to level of awareness, and the information dynamics for the part of the population at awareness level i is governed by

$$\frac{dN_i}{dt} = -\alpha \frac{N_i}{N} N_{<i} + \alpha \frac{N_{i-1}}{N} (N - N_{<i}) - \lambda(N_i - N_{i-1}),$$

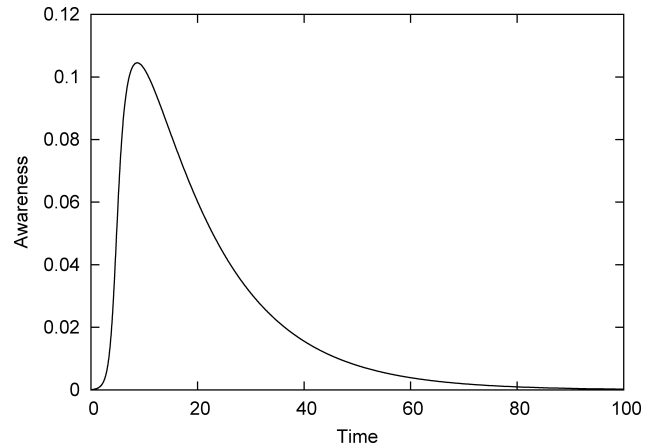


Fig. 1. Awareness $g(\rho, t)$ in the well-mixed population as a function of time for a given $\rho < 1$ if information is not replenished by the presence of the disease.

where $N_{<i} = \sum_0^{i-1} N_j$ is the number of individuals having better than i th hand information.

At any moment, awareness is then somehow distributed in the population, and this distribution changes over time according to the model dynamics. If new, and thus high-quality information is introduced once in a population in which no or only low-quality information is available, this will initially spread to increase the total amount of information in the population, given by $\sum_{i=0}^{\infty} \rho^i N_i$, only if $\alpha/\lambda > (1 - \rho)/\rho$, which ensures that sufficiently many get informed to counteract the contemporaneous loss of quality (see [supporting information \(SI Appendix\)](#)). As the quality of the information diminishes while it is passed through the population, and at the same time the population gradually forgets, the only equilibrium here is one in which information is completely absent, i.e., information always disappears eventually after an initial rise (Fig. 1). Only if first-hand information is continually refreshed by the presence of a disease, the distribution of the information reaches a nonzero equilibrium.

By linking the model of information spread with the SIR model of the spreading disease, we obtain the full set of differential equations describing the interaction between the two processes (see [SI Appendix](#)). Now, a mutual feedback between information and disease emerges: higher prevalence of the disease entails more highly informed individuals, which in turn disseminate more information into the susceptible population, thereby impeding the further spread of the disease.

We can obtain a clearer picture of this interaction by summing the equations over the information states. In that case, the mean-field equations reduce to a form similar to the SIR equations,

$$\begin{aligned} \frac{dS}{dt} &= -\beta' \frac{S}{N} I, \\ \frac{dI}{dt} &= \beta' \frac{S}{N} I - \gamma I, \\ \frac{dR}{dt} &= \gamma I, \end{aligned}$$

where $\beta'(\rho, \{S_i(t)\}) = \beta \cdot [1 - g(\rho, \{S_i(t)\})]$ reflects the current level of awareness within the susceptible population and can be interpreted as the *effective rate of infection* as part of the population is shielded by its awareness and the corresponding behavioral response. Since $\beta'(\rho, \{S_i(t)\})$ depends on the distribution of the $S_i(t)$, this system is not closed, but it is still useful for understanding the behavior at the start of an outbreak. If at any time all susceptibles were maximally aware ($S = S_0$), β' would be 0 and

the disease would not spread at all, a situation that will never arise in the model because susceptibles can at best obtain S_1 status if they are informed by infecteds with first-hand information (I_0). If, however, at any instant nobody is aware ($S \rightarrow S_\infty$), β' becomes equal to β , and the model reduces to the conventional SIR model (see, e.g., refs. 19 and 20) with infection rate β and recovery rate γ . In the conventional SIR model, the epidemic threshold is at $R_0 = \beta/\gamma = 1$, meaning that an initially low number of infecteds will increase if $\beta > \gamma$ to cause an epidemic, whereas the disease will die out if $\beta < \gamma$.

Intriguingly, in this version of our model, the epidemic threshold does not change compared with the conventional SIR model if we start with a fully uninformed and susceptible population. In that case, awareness arises only through the process of *information generation*, coupled to the parameter ω and the number of infected I . This becomes relevant only once sufficiently many carry the disease, and only then is β' reduced with respect to β . During the initial stages of the outbreak, however, $\beta' \approx \beta$, and the number of infected will always increase initially if $\beta > \gamma$. Only if a certain level of awareness were already present at the time t_0 of the beginning of the outbreak, the threshold would be reduced to $R_0 = \beta'(\rho, \{S_i(t_0)\})/\gamma$.

Even with an unchanged epidemic threshold, the outbreak ceases to grow once $S(t) = N\gamma/\beta'(\rho, \{S_i(t)\})$, which can be at a significantly lower level than the usual peak at $S = N\gamma/\beta$, and, similarly, the final size of the epidemic can be much lower than without the effect of spreading awareness (see *SI Appendix*).

Individual-Based Analysis

The analysis presented in the previous section regarded the system at the population level under the assumption of random mixing, such that both the pathogen and the different levels of awareness were each distributed homogeneously within the population. In individual-based network models, however, each member of the population is embedded into a network of contacts and can infect others only over the connections of that network. In real social networks, mixing is far from random, and the number of connections each individual forms is limited and can vary significantly (21).

In a conventional SIR model, the infection events originating from a given infected individual are realized independently with identical probability T , and the average number of secondary individuals infected by a randomly chosen individual that has been infected is given by (20, 22–24)

$$\hat{R}_0 = TD_k = T \left(\bar{k} - 1 + \frac{\text{Var}(k)}{\bar{k}} \right),$$

where \bar{k} is the average degree, or number of contacts, and $\text{Var}(k)$ is the variance thereof, such that D_k represents the effective number of contacts each individual has within the network. The basic reproductive number \hat{R}_0 defines a threshold similar to the way R_0 does in the mean-field case, in the sense that a large outbreak is possible only if every individual infects more than one other individual on average, that is if $\hat{R}_0 > 1$. In a conventional SIRS model, $T = \hat{\beta}/(\hat{\beta} + \gamma)$ (25), and the mean-field approximation is realized by taking the limit of $\bar{k} \rightarrow \infty$ while keeping $\bar{k}\hat{\beta} = \beta$ constant, yielding $\hat{R}_0 \rightarrow R_0 = \beta/\gamma$.

Here, we will first consider the case where disease spreads locally, but information is disseminated globally, as in the case where awareness is triggered by information broadcast through the media. If the spread of information is well-described by the mean-field approximation presented above, we can assume that information quality is independent and identically distributed within susceptible contacts of infected individuals. In that case,

the probability of infection at time t over a given link chosen at random is

$$T'(t) = \sum_{i=1}^{\infty} p_i(t) T_i \quad \text{with} \quad T_i = \frac{\hat{\beta}(1 - \rho^i)}{\hat{\beta}(1 - \rho^i) + \gamma},$$

where $p_i(t)$ is the probability of the susceptible at risk of infection to possess information having gone through i hands at time t , and T_i is the probability of infection of that neighbor. If the distribution of awareness is already present at the time t_0 of the beginning of an outbreak the basic reproductive number is reduced to

$$\hat{R}'_0 = T'(t_0) D_k = \hat{R}_0 - (T - T'(t_0)) D_k.$$

In the limit of random mixing of disease contacts, this reduces to $\hat{R}'_0 \rightarrow \hat{R}'_0 = \beta'(\rho, t_0)/\gamma$ as found in our mean-field analysis.

A completely different picture emerges if awareness, just like the disease, is not just globally present but spreads locally from individual to individual during the initial stages of the outbreak. Before we look at the full picture, let us assume for the moment that information transmission is only occurring between infected individuals informing their susceptible contacts, but that the information is not passed on any further, which could be regarded as analogous to single-step contact tracing. In that case, the impact of awareness depends on the number of edges emanating from each node that are common to both networks. If we let (kc) denote the common degree, that is the number of contacts for possible disease transmission that are also information contacts, and (kd) the degree for contacts of disease transmission only, the reduced basic reproductive number is given by

$$\hat{R}'_0 = T'D_{(kc)} + T_\infty D_{(kd)} \quad T' = p_0 T_0 + p_1 T_1,$$

where $T_\infty = \hat{\beta}/(\hat{\beta} + \gamma)$ is the transmission probability to completely uninformed individuals, as the contacts of information transmission leading to individuals not at risk of disease transmission do not contribute to the reduction of \hat{R}_0 . In this approximation, we can derive a full expression for the reduced transmission probability T' in terms of the information-related quantities ω , $\hat{\alpha}$, and ρ (see *SI Appendix*). As a consequence of the reduction in T' , the basic reproductive number \hat{R}'_0 is lower than \hat{R}_0 and can drop below the threshold of $\hat{R}'_0 = 1$ even if $\hat{R}_0 > 1$, in which case the disease is prevented from growing into an epidemic, unlike it would do without the effect of spreading awareness. Given the information-related parameters, we can derive a *critical* value $\hat{R}_0^{\text{crit}}(\hat{\alpha}, \omega, \rho)$ of the basic reproductive number of the disease, in the sense that information can in principle prevent it from taking hold in the population if $\hat{R}_0 < \hat{R}_0^{\text{crit}}$ (see *SI Appendix*).

While the full expression for this critical \hat{R}_0^{crit} is complex and does not lend itself to a simple interpretation, we can gain insight into the underlying principles by deriving upper bounds on that critical level. The protection provided by being informed is constrained by the value of the decay constant ρ . Consequently, if \hat{R}_0 is greater than

$$\lim_{\substack{\omega \rightarrow \infty \\ \hat{\alpha} \rightarrow \infty}} \hat{R}_0^{\text{crit}} = \frac{1}{1 - \rho(1 - D_k^{-1})},$$

for a given disease, there is no chance for local information to stop the disease from growing into an epidemic, however fast it is generated and spreads within the population (Fig. 2).

Even if ρ is large, information needs to be both generated and spread at a sufficiently high rate to have an effect on the disease outbreak. Given either the rate of information generation ω , or the rate of information spread $\hat{\alpha}$, we can determine two more

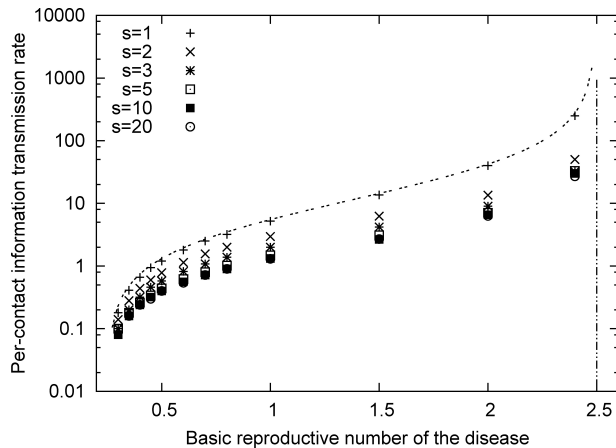


Fig. 2. Per contact information transmission rate $\hat{\alpha}$ needed to push the outbreak below the epidemic threshold for a given basic reproductive number of the disease \hat{R}_0 . Shown is the theoretical prediction (line) and simulation results for different values of s , the number of steps information is allowed to travel from the source. The nodes were connected as a random regular graph, i.e., randomly with uniform degree $k = 6$, and the data points closely follow the predicted line. The critical \hat{R}_0^{crit} for the parameters used here ($\rho = 0.9$) is indicated by a vertical line.

upper bounds on the critical value of the basic reproductive number beyond which the disease cannot be stopped from reaching epidemic proportions:

$$\lim_{\omega \rightarrow \infty} \hat{R}_0^{\text{crit}} = \frac{\gamma + \hat{\alpha}}{\gamma + \hat{\alpha} D_k^{-1}} \quad \text{and} \quad \lim_{\hat{\alpha} \rightarrow \infty} \hat{R}_0^{\text{crit}} = \frac{\gamma + \omega}{\gamma + \omega D_k^{-1}},$$

represent situations where any information transmission or information generation, respectively, would fully protect the informed individual from getting infected. If all the parameters of information spread are given, these three limits all represent upper bounds for the critical reproductive number \hat{R}_0^{crit} , significantly limiting the potential impact of local information spread on the epidemic threshold. Only through a proper combination of all three involved processes (information generation, transmission, and protection) can the basic reproductive number be altered significantly.

The full effect of the interaction between the two spreading processes comes into play when we let the information propagate independently without limiting the number of steps it can spread. In that case, there is a chance for an infected individual to have its susceptible contacts informed through others, and T' can be further reduced. However, there remains a limit to the effect as the first upper bound on \hat{R}_0^{crit} remains in place if $\rho < 1$ (Fig. 2). Only if information is perfect and individuals completely remove themselves from the epidemic system when they are informed can any disease be stopped.

A way to push that limit toward higher values of \hat{R}_0 even without the need for perfect protection would be for individuals to rewire their contacts dynamically (see, e.g., ref. 17), i.e. to cut a transmissive contact to the person they have just been informed by and establish a contact to another person instead. In that case, \hat{R}'_0 can indeed be shown to be reduced further, although it remains a mild effect as it affects only contacts that are common to the disease and information networks.

The reduction in the basic reproductive number and its limits are clearly a consequence of the contact-based view, and they did not appear in the mean-field analysis. In fact, the mean-field limit of the full expression for \hat{R}'_0 still yields $\hat{R}'_0 \rightarrow R_0 = \beta/\gamma$. With respect to the well-mixed scenario, the existence of edges that are common to both networks introduced

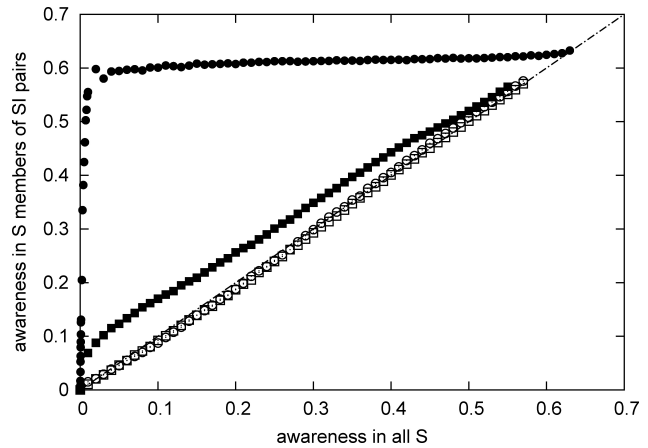


Fig. 3. Average awareness in the susceptible members of SI pairs in terms of the average awareness in all susceptibles, measured in stochastic simulations on the following scenarios of disease and information network structure: completely overlapping (filled squares) and completely disjointed (open squares) regular random graphs, completely overlapping lattices (filled circles) and the disease network as a lattice with the information network as a regular random graph (open circles). The line corresponds to the case $p_i^{\text{SI}} = p_i^S$.

an element of structure that has no equivalent in the mean-field approximation.

Network Overlap

The single-step analysis presented in the previous section allowed for the two networks to be different, in that contacts of infectious individuals on the disease network that were not connected to the same individual on the information network were assumed to be completely unprotected. However, if awareness is allowed to spread for more than just one step, such missing links can partially be compensated for if there are other paths connecting an infected individual and its susceptible neighbor, i.e., if information links are clustered around the disease links.

Ultimately, the influence of spreading awareness on a disease outbreak depends on how much the individuals at the front of the growing epidemic are aware of its presence. Although the impact of heterogeneities in the degree distribution [including so-called scale-free network topologies (26)] can be captured in the factors $D_{(kc)}$ and $D_{(kd)}$, other properties of the two networks and their relation to each other can have a strong impact on the containment of the disease. Going back to a deterministic description of the system, we can get some insight into the relevant processes and their dependence on network structure and overlap by considering the dynamics of the population-level variables in terms of pairs (27). Denoting the number of pairs of a given type on the disease network with $[...]^d$, the equation for the number of infected individuals contains a term

$$I = \dots + \hat{\beta} \sum_{i=0}^{\infty} (1 - \rho^i) [S_i I]^d \dots,$$

which can be rewritten as

$$\dot{I} = \dots + \hat{\beta} \sum_{i=0}^{\infty} ((1 - \rho^i) p_i^{\text{SI}}) [SI]^d \dots$$

Here, $p_i^{\text{SI}} = [S_i I]^d / [SI]^d$ represents the probability that the S member in a randomly chosen SI pair on the disease network to be at information level i , such that $\hat{\beta}' = \hat{\beta} \sum (1 - \rho^i) p_i^{\text{SI}}$, can be regarded as the analogue to the effective infection rate β' of the mean-field equations. If no correlation exists between the locations of disease and information and they spread completely independently, the p_i^{SI} are given by



Fig. 4. Snapshot of a simulated disease outbreak on a triangular lattice. Red represents nodes that have been infected during the outbreak, with light red indicates nodes that are still spreading the disease. Darker shades of gray correspond to higher levels of awareness in susceptibles. Animated versions are available as supporting video. (See *SI Appendix*, Movies S1 and S2).

$$p_i^{SI} = p_i^S = S_i/S$$

which is nothing but the probability of a randomly chosen susceptible to be at information level i . If this equation holds, no correlation exists between information level and risk of catching the disease, and the effect of awareness is again one of a homogeneously distributed reduction in susceptibility.

Although it is not practical to derive an analytical expression for the behavior of p_i^{SI} in terms of network structure and overlap, we can measure it on simulated networks. In Fig. 3, one sees that if the information network is connected randomly and independently of the disease network, we obtain the mean-field situation where $p_i^{SI} = p_i^S$. If both networks are connected randomly but coincide, information is distributed more effectively and we observe a mild departure from equality of p_i^{SI} and p_i^S . A much more pronounced effect, however, can be observed if the two networks are triangular lattices, which contain many clusters, or triangles of connections. In that case, information is distributed much more effectively if the two networks coincide, resulting in significant correlation between risk of infection and information level, such that that much less total information is needed to protect the part of the population most at risk. Fig. 4 illustrates this effect, showing a snapshot of a simulated disease outbreak with awareness spreading on an triangular lattice completely overlapping with the disease network. Clouds of information have already formed around infected individuals, strongly limiting the further spread of the disease.

Discussion

On a social network, spreading awareness of a contagious disease in conjunction with a reduction in susceptibility does not only

lower the incidence of that disease, but in some cases can even prevent that disease from growing into an epidemic. This is the case even if the awareness is not triggered by central information, but instead based on information that is passed on from person to person. However, beyond a critical infection rate, spreading awareness can slow down the spread of a disease and lower the final incidence, but it cannot completely stop it from reaching epidemic proportions and taking over large parts of the population. Only if the disease is easily recognized and information spreads rapidly, while at the same time there is a strong tendency toward protective behavior, awareness of a disease outbreak can bring the infection rate of a disease down significantly. If all of these factors work together, rapid drops in the transmissibility of a disease, as have been observed, for example, in the 2003 outbreak of SARS in Hong Kong (28), might be rooted in processes similar to the ones here presented.

Social network structure is found to play a significant role in the way spreading awareness and a contagious disease interact. The relative clustering of the information network around infectious individuals determines how effectively spreading awareness can constrain an epidemic outbreak. This effectiveness is significantly lowered when the network of disease spread differs from the communication network. This could be of relevance in the case of sexually transmitted disease, where a strong heterogeneity in the relevant network has been observed (29) and highly sexually active individuals are of crucial importance, yet do not necessarily find themselves in the same parts of the communication network as potential infectious contacts (e.g., sex workers might not communicate frequently with their customers). However, contact tracing programs work exactly to bring the two networks to match and can be seen as a special case of overlapping networks with just one step of information transmission.

Because the presence of a disease can change human behavior, care should be taken when trying to predict disease progression from behavioral observations in populations where the disease is not present (30, 31) or from observations on a different disease (32). Our model suggests how the interaction of social network structure with the properties of the disease induces a change in behavior in individuals and our results show how this could feed back to alter the disease dynamics.

Up to now, the effects of social distancing have predominantly been studied from a viewpoint of centrally controlled action. We argue that it is of equal importance to consider the self-initiated reactions of individuals in the presence of a contagious disease. The model we analyzed here differs from the previous studies of the effect of social distancing in that we treat it as a local effect within the population which depends on the awareness of the social proximity of a disease. The importance of this is particularly relevant but not limited to cases like SARS in China where initially no information was made available by the governing bodies. Therefore, we think this can provide a valuable contribution to the ongoing discussion about the impact to be expected from social distancing in disease outbreaks to come.

ACKNOWLEDGMENTS. This work was supported by UK Engineering and Physical Sciences Research Council Grant EP/D002249/1.

1. Ferguson N (2007) Capturing human behaviour. *Nature* 446:733.
2. Philipson T (1996) Private vaccination and public health: An empirical examination for U.S. measles. *J Hum Resour* 31:611–630.
3. Ahiatu A, Hotz VJ, Philipson T (1996) The responsiveness of the demand for condoms to the local prevalence of AIDS. *J Hum Resour* 31:896–897.
4. Macintyre K, Brown L, Sosler S (2001) "It's not what you know, but who you knew": Examining the relationship between behavior change and AIDS mortality in Africa. *AIDS Edu Prev* 13:160–174.
5. Tai Z, Sun T (2007) Media dependencies in a changing media environment: The case of the 2003 SARS epidemic in China. *New Media Soc* 9:987–1010.
6. World Health Organization (2003) *Consensus Document on the Epidemiology of SARS* (World Health Organization, Geneva, Switzerland).
7. Nekovee M, Moreno Y, Bianconi G, Marsili M (2007) Theory of rumour spreading in complex social networks. *Physica A* 374:457–470.
8. Lynch A (1991) Thought contagion as abstract evolution. *J Ideas* 2:3–10.
9. Goffman W, Newill VA (1964) Generalization of epidemic theory: An application to the transmission of ideas. *Nature* 204:225–228.
10. Agliari E, Burioni R, Cassi D, Neri FM (2006) Efficiency of information spreading in a population of diffusing agents. *Phys Rev E* 73:046138.
11. Hatchett RJ, Mecher CE, Lipsitch M (2007) Public health interventions and epidemic intensity during the 1918 influenza pandemic. *Proc Natl Acad Sci USA* 104: 7582–7587.
12. Bootsma MCJ, Ferguson NM (2007) The effect of public health measures on the 1918 influenza pandemic in U.S. cities. *Proc Natl Acad Sci USA* 104:7588–7593.

13. Bauch CT, Galvani AP, Earn DJD (2003) Group interest versus self-interest in smallpox vaccination policy. *Proc Natl Acad Sci USA* 100:10564–10567.
14. Perisic A, Bauch CT (2009) Social contact networks and disease eradicability under voluntary vaccination. *PLoS Comput Biol* 5:e1000280.
15. Galvani AC, Reluga TC, Chapman GB (2007) Long-standing influenza vaccination policy is in accord with individual self-interest but not with the utilitarian optimum. *Proc Natl Acad Sci USA* 104:5692–5697.
16. Salathé M, Bonhoeffer S (2008) The effect of opinion clustering on disease outbreaks. *J R Soc Interface* 5:1505–1508.
17. Gross I, D'Lima CJD, Blasius B (2006) Epidemic dynamics on an adaptive network. *Phys Rev Lett* 96:208701.
18. Del Valle S, Hethcote H, Hyman JM, Castillo-Chavez C (2005) Effects of behavioral changes in a smallpox attack model. *Math Biosci* 195:228–251.
19. Anderson RM, May RM (1991) Infectious Diseases of Humans: Dynamics and Control. (Oxford Univ Press, Oxford).
20. Diekmann O, Heesterbeek JAP (2000) *Mathematical Epidemiology of Infectious Diseases* (Wiley, Chichester, UK).
21. Eubank S, et al. (2004) Modelling disease outbreaks in realistic urban social networks. *Nature* 429:180–184.
22. Anderson RM, Medley GF, May RM, Johnson AM (1986) A preliminary study of the transmission dynamics of the human immunodeficiency virus (HIV), the causative agent of AIDS. *IMA J Math Appl Med Biol* 3:229–263.
23. Andersson H (1997) Epidemics in a population with social structures. *Math Biosci* 140:79–84.
24. Meyers LA (2007) Contact network epidemiology: Bond percolation applied to infectious disease prediction and control. *Bull Am Math Soc* 44:63–86.
25. Keeling MJ, Grenfell BT (2000) Individual-based perspectives on R_0 . *J Theor Biol* 203:51–61.
26. Barabási AL, Albert R (1999) Emergence of scaling in random networks. *Science* 286:509–512.
27. Keeling MJ (1999) The effects of local spatial structure on epidemiological invasions. *Proc R Soc Lond B* 266:859–867.
28. Riley S, et al. (2003) Transmission dynamics of the etiological agent of SARS in Hong Kong: Impact of public health interventions. *Science* 300:1961–1966.
29. Liljeros F, Edling CR, Amaral LAN, Stanley HE, Åberg Y (2001) The web of human sexual contacts. *Nature* 411:707–708.
30. Mossong J, et al. (2008) Social contacts and mixing patterns relevant to the spread of infectious diseases. *PLoS Med* 5:381–391.
31. Edmunds WJ, O'Callaghan CJ, Nokes DJ (1997) Who mixes with whom? A method to determine the contact patterns of adults that may lead to the spread of airborne infections. *Proc R Soc Lond B* 264:949–957.
32. Reyes F, et al. (2008) Influenza in Canada: 2007–2008 season update. *Can Commun Dis Rep* 34:1–9.

Supplementary material

The spread of awareness and its impact on epidemic outbreaks

Sebastian Funk, Erez Gilad, Chris Watkins, Vincent A.A. Jansen

In the following, we will present and analyze the system of ordinary differential equations describing the mean-field dynamics, and carry out the calculations leading to the basic reproductive number in the individual-based model.

Mean-field analysis

Subscript i denotes information at the i -th generation, i.e. diminished times by a factor ρ . Subscript 0 denotes the 0-th generation, information which has not been transmitted or lost quality yet. Disregarding the generation of information for the moment by setting $\omega = 0$, the full set of mean-field equations is

$$\frac{dS_i}{dt} = -(1 - \rho^i)\beta \frac{S_i}{N} I - \alpha \frac{S_i}{N} \left(\sum_{j=0}^{i-2} N_j \right) + \alpha \frac{N_{i-1}}{N} \left(\sum_{j=i+1}^{\infty} S_j \right) - \lambda S_i + \lambda S_{i-1}, \quad (1)$$

$$\frac{dI_i}{dt} = +(1 - \rho^i)\beta \frac{S_i}{N} I - \gamma I_i - \alpha \frac{I_i}{N} \left(\sum_{j=0}^{i-2} N_j \right) + \alpha \frac{N_{i-1}}{N} \left(\sum_{j=i+1}^{\infty} I_j \right) - \lambda I_i + \lambda I_{i-1}, \quad (2)$$

$$\frac{dR_i}{dt} = +\gamma I_i - \alpha \frac{R_i}{N} \left(\sum_{j=0}^{i-2} N_j \right) + \alpha \frac{N_{i-1}}{N} \left(\sum_{j=i+1}^{\infty} R_j \right) - \lambda R_i + \lambda R_{i-1}, \quad (3)$$

where $I = \sum_i I_i$ and $N_i = S_i + I_i + R_i$, and $S_{-1} = I_{-1} = R_{-1} = N_{-1} = 0$. The dynamical equation for I is

$$\frac{dI}{dt} = \sum_i \frac{dI_i}{dt} = + \left(\sum_{i=0}^{\infty} (1 - \rho^i) \beta \frac{S_i}{N} \right) I - \gamma I \quad (4)$$

and the initial rate of increase of infected starting with a small number of infected in an otherwise completely susceptible and uninformed population is $\exp(\beta - \gamma)t$, such that initially number of infected will always increase if $\beta/\gamma > 1$.

Disease dynamics

Rephrasing the system in terms of the dynamical variables $S = \sum_i S_i$, $I = \sum_i I_i$ and $R = \sum_i R_i$ reduces the system to SIR dynamics:

$$\frac{dS}{dt} = -\beta'(\rho, t) \frac{S}{N} I, \quad (5)$$

$$\frac{dI}{dt} = \beta'(\rho, t) \frac{S}{N} I - \gamma I, \quad (6)$$

$$\frac{dR}{dt} = \gamma I, \quad (7)$$

in which $\beta'(\rho, t) = \beta(1 - g(\rho, t))$, and $g(\rho, t)$ is the probability generating function of the distribution of information among susceptibles at time t , $g(\rho, t) = \sum_i (S_i(t)/S(t)) \rho^i$, $i = 0, 1, 2, \dots$

Information dynamics

Rephrasing the system in terms of the N_i yields the information dynamics (if $\omega = 0$):

$$\begin{aligned}\frac{dN_i}{dt} &= -\alpha \frac{N_i}{N} \left(\sum_{j=0}^{i-1} N_j \right) + \alpha \frac{N_{i-1}}{N} \left(N - \sum_{j=0}^{i-1} N_j \right) - \lambda N_i + \lambda N_{i-1} \\ &= -\alpha \frac{N_i}{N} N_{<i} + \alpha \frac{N_{i-1}}{N} (N - N_{<i}) - \lambda (N_i - N_{i-1}),\end{aligned}\quad (8)$$

where $N_{<i} = \sum_{j=0}^{i-1} N_j$ is the sum over all more informed parts of the population. In equilibrium, we have

$$N_i = \frac{1 + \frac{\alpha}{\lambda} \frac{N - N_{<i}}{N}}{1 + \frac{\alpha}{\lambda} \frac{N_{<i}}{N}} N_{i-1},$$

for all $i > 0$. Therefore, the condition for the maximum of the distribution of information is

$$N_{<1} = \frac{1}{2} N,$$

such that, in equilibrium, the maximum of the distribution is always its median. The total amount of information in the population, $Q = \sum_{i=0}^{\infty} \rho^i N_i$ changes in time as

$$\begin{aligned}\frac{dQ}{dt} &= -\frac{\alpha}{N} \sum_{i=0}^{\infty} \sum_{j=0}^{i-1} \rho^i N_i N_j + \frac{\alpha}{N} \sum_{i=0}^{\infty} \rho^i N_{i-1} N - \frac{\alpha}{N} \sum_{i=0}^{\infty} \sum_{j=0}^{i-1} \rho^i N_{i-1} N_j - \lambda \sum_{i=0}^{\infty} \rho^i (N_i - N_{i-1}) \\ &= -(1 + \rho) \frac{\alpha}{N} \sum_{i=1}^{\infty} \rho^i N_i N_{<i} + \alpha \rho Q - \lambda (1 - \rho) Q,\end{aligned}\quad (11)$$

and the initial rate of increase of awareness starting with a small number of informed in an otherwise completely uninformed population is $\alpha\rho - \lambda(1 - \rho)$. Hence, awareness in the population will increase if

$$\frac{\rho}{(1 - \rho)} \frac{\alpha}{\lambda} > 1.$$

Information generation

The inclusion of information generation into the model adds the following terms:

$$\begin{aligned}\frac{dI_0}{dt} &= \dots + \omega(I - I_0) \\ \frac{dI_{>0}}{dt} &= \dots - \omega I_i,\end{aligned}\quad (13)$$

which do not change the disease equations.

With information generation, the dynamical equation for the most informed part of the population N_0 is

$$\frac{dN_0}{dt} = -\lambda N_0 + \omega(I - I_0).\quad (14)$$

Note that, however, $S_0 = 0$ at all times as susceptibles will always have their information passed on to them by someone.

Final sizes

Examples of the possible reduction in the final size of the outbreak are given in Supporting Figures 1-3, which show the fraction of the population having been infected by the end of an outbreak as calculated from the ODE system in terms of the information transmission rate α for different values of the decay constant ρ and the rate of information generation ω .

Individual-based analysis

In our individual-based model, every individual has a number of contacts with other individuals, distributed with mean \bar{k} and variance $\text{Var}(k)$. Each of these contacts have independent probability of disease transmission, in case one of the two individuals at its ends is infected and the other susceptible. Given the average transmission probability T and the distribution of the number of contacts each individual possesses, the average number of secondary infections caused by an infected individual is called the *basic reproductive number* \hat{R}_0 . In a conventional SIR model on a network, it is given by [1; 2; 3; 4]

$$\hat{R}_0 = TD_k = \frac{\hat{\beta}}{\hat{\beta} + \gamma} D_k \quad (15)$$

where $T = \hat{\beta}/(\hat{\beta} + \gamma)$ is the per-contact probability of infection [5] (or the probability that infection happens before recovery) and

$$D_k = \left(\bar{k} - 1 + \frac{\text{Var}(k)}{\bar{k}} \right) \quad (16)$$

takes into account the variation in the number of contacts each individual has.

In our model, variation in the state of awareness of susceptibles changes the transmission probabilities. If the susceptible contact at the end of a connection for potential disease transmission is in awareness state i , the transmission probability for a given contact between a susceptible and an infected is given by

$$T_i = \frac{\hat{\beta}(1 - \rho^i)}{\hat{\beta}(1 - \rho^i) + \gamma}, \quad (17)$$

and the modified basic reproductive number by

$$\hat{R}'_0 = \left(\sum_{i=1}^{\infty} p_i T_i \right) D_k \quad (18)$$

where p_i is the probability of the susceptible to possess information having gone through i hands at the time of potential infection, and T_i is the probability of infection over that contact given that i .

If we restrict ourselves to one-step of information transmission, only the transmission probabilities p_0 and p_1 are non-zero. In fact, p_0 is the probability that infection or recovery happens before information is generated plus the probability that, if information is generated before infection or recovery happens, one of the two still occurs before information is transmitted. Therefore, we have

$$p_0 = \frac{\hat{\beta} + \gamma}{\hat{\beta} + \gamma + \omega} + \frac{\omega}{\hat{\beta} + \gamma + \omega} \frac{\hat{\beta} + \gamma}{\hat{\beta} + \gamma + \hat{\alpha}} \quad (19)$$

$$p_1 = \frac{\omega}{\hat{\beta} + \gamma + \omega} \frac{\hat{\beta} + \gamma + \hat{\alpha}}{\hat{\beta} + \gamma + \hat{\alpha}} \quad (20)$$

To assess the maximum impact the information process can have on the spreading disease, let us assume the networks for the spread of awareness and the disease to be the same. The modified basic reproductive number, $\hat{R}'_0 = (p_0 \hat{R}_0 + p_1 \hat{R}_1) D_k$ is then given by

$$\begin{aligned} \hat{R}'_0 &= \left(\left(\frac{\hat{\beta} + \gamma}{\hat{\beta} + \gamma + \omega} + \frac{\omega}{\hat{\beta} + \gamma + \omega} \frac{\hat{\beta} + \gamma}{\hat{\beta} + \gamma + \hat{\alpha}} \right) \frac{\hat{\beta}}{\hat{\beta} + \gamma} + \frac{\omega}{\hat{\beta} + \gamma + \omega} \frac{\hat{\alpha}}{\hat{\beta} + \gamma + \omega} \frac{\hat{\beta}(1 - \rho)}{\hat{\beta}(1 - \rho) + \gamma} \right) D_k \\ &= \left(\frac{\hat{\beta}}{\hat{\beta} + \gamma + \omega} + \frac{\omega}{\hat{\beta} + \gamma + \omega} \frac{\hat{\beta}}{\hat{\beta} + \gamma + \hat{\alpha}} + \frac{\omega}{\hat{\beta} + \gamma + \omega} \frac{\hat{\alpha}}{\hat{\beta} + \gamma + \omega} \frac{\hat{\beta}(1 - \rho)}{\hat{\beta}(1 - \rho) + \gamma} \right) D_k \\ &= \left(\frac{\hat{\beta}}{\hat{\beta} + \gamma + \omega} \left(1 + \frac{\omega}{\hat{\beta} + \gamma + \hat{\alpha}} \left(1 + \frac{(1 - \rho)\hat{\alpha}}{(1 - \rho)\hat{\beta} + \gamma} \right) \right) \right) D_k \\ &= \left(\frac{\hat{\beta} + \gamma}{\hat{\beta} + \gamma + \omega} \left(1 + \frac{\omega}{\hat{\beta} + \gamma + \hat{\alpha}} \left(1 + \frac{(1 - \rho)\hat{\alpha}}{(1 - \rho)\hat{\beta} + \gamma} \right) \right) \right) \hat{R}_0 \end{aligned} \quad (21)$$

The mean-field limit is taken by setting $\bar{k} \rightarrow \infty$, $\hat{\alpha} \rightarrow 0$, $\hat{\beta} \rightarrow 0$, $\bar{k}\hat{\alpha} \rightarrow \alpha$, and $\bar{k}\hat{\beta} \rightarrow \beta$. In that case, we get $\hat{R}'_0 \rightarrow R_0 = \frac{\beta/\gamma}{\hat{\beta}/\gamma}$.

Solving $\hat{R}'_0 = 1$ for \hat{R}_0 yields

$$\begin{aligned}\hat{R}_0^{\text{crit}} &= \frac{(\hat{\beta} + \gamma + \omega)(\hat{\beta} + \gamma + \hat{\alpha})(1 - \rho)\hat{\beta} + \gamma)}{(\hat{\beta} + \gamma)\left[(\hat{\beta} + \gamma + \omega + \hat{\alpha})(1 - \rho)\hat{\beta} + \gamma) + \omega\hat{\alpha}(1 - \rho)\right]} \\ &= 1 + \frac{(\hat{\beta} + \gamma)\left[(\hat{\beta} + \gamma + \omega + \hat{\alpha})((1 - \rho)\hat{\beta} + \gamma) + \omega\hat{\alpha}(1 - \rho)\right]}{\omega\alpha(1 - \rho)\gamma}\end{aligned}\quad (22)$$

The following limits can be applied to Eq. 21 before solving for \hat{R}_0 :

$$\lim_{\hat{\beta} \rightarrow \infty} \hat{R}_0^{\text{crit}} = 1, \quad (23)$$

and, using $\hat{\beta} = \gamma\hat{R}_0^{\text{crit}}/(D_k - \hat{R}_0^{\text{crit}})$ (Eq. 15)

$$\lim_{\substack{\omega \rightarrow \infty \\ \hat{\alpha} \rightarrow \infty}} \hat{R}_0^{\text{crit}} = \frac{1}{1 - \rho(1 - D_k^{-1})}, \quad (24)$$

$$\lim_{\substack{\omega \rightarrow \infty \\ \rho \rightarrow 1}} \hat{R}_0^{\text{crit}} = \frac{\gamma + \hat{\alpha}}{\gamma + \hat{\alpha}D_k^{-1}}, \quad (25)$$

$$\lim_{\substack{\hat{\alpha} \rightarrow \infty \\ \rho \rightarrow 1}} \hat{R}_0^{\text{crit}} = \frac{\gamma + \omega}{\gamma + \omega D_k^{-1}}. \quad (26)$$

References

- [1] Anderson RM, Medley GF, May RM, Johnson AM (1986) A preliminary study of the transmission dynamics of the human immunodeficiency virus (HIV), the causative agent of AIDS. *IMA J Math Appl Med Biol* 3:229–263. 136–142.
- [2] Andersson H (1997) Epidemics in a Population with Social Structures. *Math Biosci* 140:79–84.
- [3] Diekmann O, Heesterbeek JAP (2000) Mathematical Epidemiology of Infectious Diseases. (Wiley, Chichester).
- [4] Meyers LA (2007) Contact Network Epidemiology: Bond Percolation Applied to Infectious Disease Prediction and Control. *Bull Amer Math Soc* 44:63–86.
- [5] Keeling MJ, Grenfell BT (2000) Individual-based Perspectives on R_0 . *J Theor Biol* 203:51–61.

Supporting Videos

Video 1

Simulated outbreak of just a disease spreading without associated awareness on a triangular lattice. Red color indicates nodes which have been infected, with brighter red indicating those that are still infectious. Darker shades of gray indicate higher levels of awareness.

Video 2

Simulated outbreak of a disease with associated awareness spreading on a triangular lattice. Red color indicates nodes which have been infected, with brighter red indicating those that are still infectious. Darker shades of gray indicate higher levels of awareness.

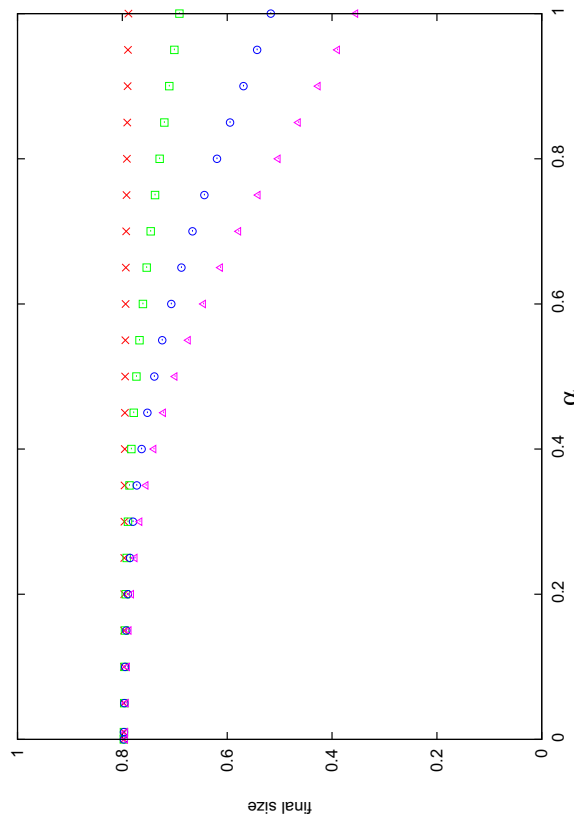


Fig. S1. Fraction of the population having been infected by the end of an outbreak as calculated from the ODE system in terms of the information transmission rate α . Different values of the decay constant ρ are indicated as crosses ($\rho = 0.5$), squares ($\rho = 0.8$), circles ($\rho = 0.9$), and triangles ($\rho = 0.95$); the rate of information generation ω is 0.01; the other parameters are $\beta = 1$, $\gamma = 0.5$, and $\lambda = 0.5$.

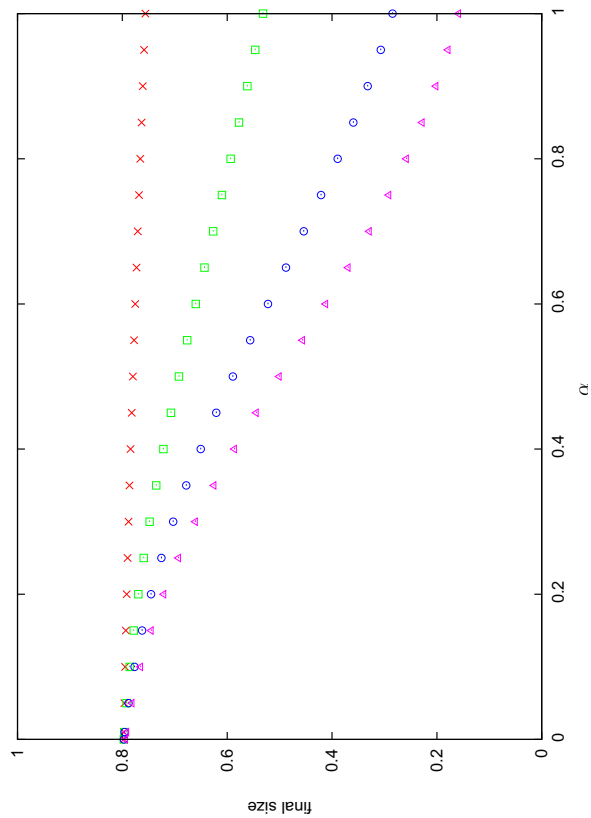


Fig. S2. Fraction of the population having been infected by the end of an outbreak as calculated from the ODE system in terms of the information transmission rate α . Different values of the decay constant ρ are indicated as crosses ($\rho = 0.5$), squares ($\rho = 0.8$), circles ($\rho = 0.9$), and triangles ($\rho = 0.95$); the rate of information generation ω is 0.1; the other parameters are $\beta = 1$, $\gamma = 0.5$, and $\lambda = 0.5$.

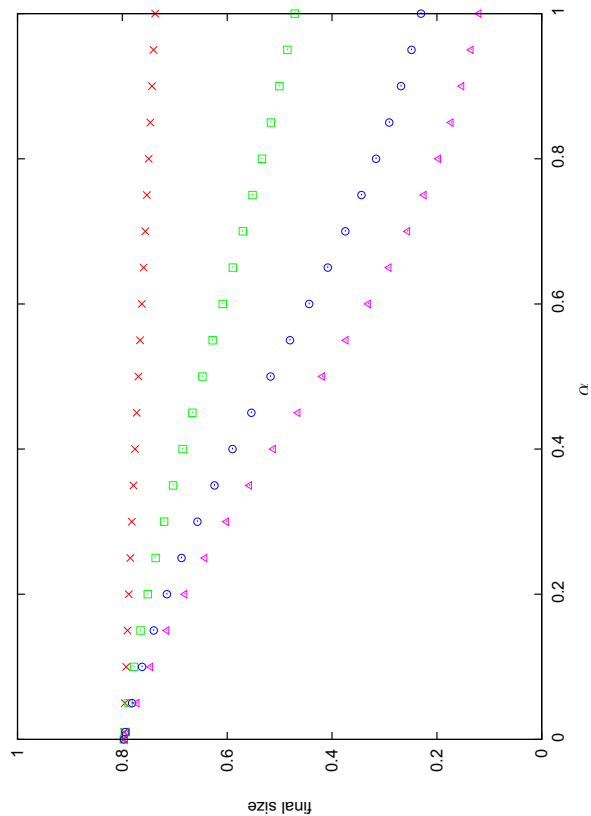
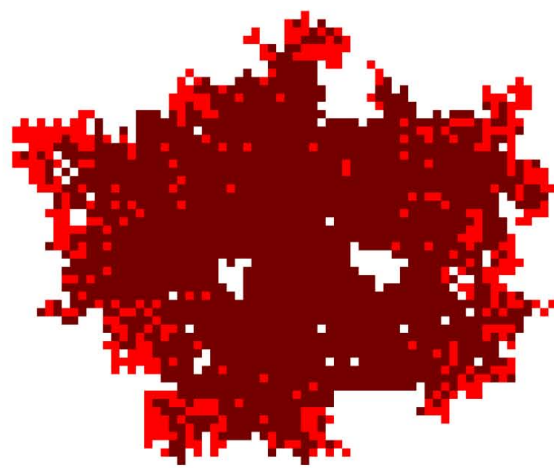
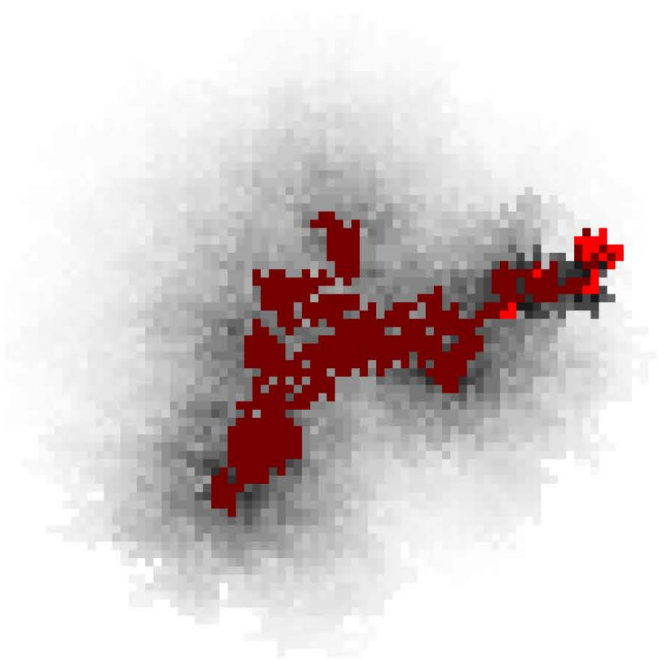


Fig. S3. Fraction of the population having been infected by the end of an outbreak as calculated from the ODE system in terms of the information transmission rate α . Different values of the decay constant ρ are indicated as crosses ($\rho = 0.5$), squares ($\rho = 0.8$), circles ($\rho = 0.9$), and triangles ($\rho = 0.95$); the rate of information generation ω is 0.2; the other parameters are $\beta = 1$, $\gamma = 0.5$, and $\lambda = 0.5$.



Movie S1. Simulated outbreak of only a disease spreading on a triangular lattice. Red color indicates nodes that have been infected, with brighter red indicating those that are still infectious.

[Movie S1 \(MOV\)](#)



Movie S2. Simulated outbreak of a disease with associated awareness spreading on a triangular lattice. Red color indicates nodes that have been infected, with brighter red indicating those that are still infectious. Darker shades of gray indicate higher levels of awareness.

[Movie S2 \(MOV\)](#)

Measuring the impact of Ebola control measures in Sierra Leone

Adam J. Kucharski¹, Anton Camacho, Stefan Flasche, Rebecca E. Glover, W. John Edmunds, and Sebastian Funk

Centre for the Mathematical Modelling of Infectious Diseases, Department of Infectious Disease Epidemiology, London School of Hygiene & Tropical Medicine, London WC1E 7HT, United Kingdom

Edited by Burton H. Singer, University of Florida, Gainesville, FL, and approved September 10, 2015 (received for review May 5, 2015)

Between September 2014 and February 2015, the number of Ebola virus disease (EVD) cases reported in Sierra Leone declined in many districts. During this period, a major international response was put in place, with thousands of treatment beds introduced alongside other infection control measures. However, assessing the impact of the response is challenging, as several factors could have influenced the decline in infections, including behavior changes and other community interventions. We developed a mathematical model of EVD transmission, and measured how transmission changed over time in the 12 districts of Sierra Leone with sustained transmission between June 2014 and February 2015. We used the model to estimate how many cases were averted as a result of the introduction of additional treatment beds in each area. Examining epidemic dynamics at the district level, we estimated that 56,600 (95% credible interval: 48,300–84,500) Ebola cases (both reported and unreported) were averted in Sierra Leone up to February 2, 2015 as a direct result of additional treatment beds being introduced. We also found that if beds had been introduced 1 month earlier, a further 12,500 cases could have been averted. Our results suggest the unprecedented local and international response led to a substantial decline in EVD transmission during 2014–2015. In particular, the introduction of beds had a direct impact on reducing EVD cases in Sierra Leone, although the effect varied considerably between districts.

Ebola virus disease | Sierra Leone | control measures | treatment beds | mathematical model

The 2013–2015 Ebola virus disease (EVD) epidemic in West Africa has seen more cases than all past outbreaks combined (1), and has triggered a major international response. In Sierra Leone, where there have been over 8,600 confirmed cases reported as of 2015 August 1, the Sierra Leone and UK governments and nongovernmental organizations have supported the gradual introduction of over 1,500 beds in Ebola Holding Centers (EHCs) and Community Care Centers (CCCs), as well as over 1,200 beds in larger-scale Ebola Treatment Units (ETUs) (2, 3). As well as the humanitarian value of providing treatment and care to sick patients, there is a secondary benefit to expanding bed capacity that is more difficult to quantify; by isolating the ill and removing them from the community, further infections might be prevented.

Since the peak of the epidemic in Sierra Leone in November 2014, when there were over 500 confirmed EVD cases reported per week, the level of infection has dropped, with fewer than 100 confirmed cases reported per week in February 2015. Although the nationwide decline in cases coincided with an increase in the number of beds available (4), as well as improved case detection, tracing of contacts, and safe burials of patients who had died (3, 5), there has been criticism of the timing and focus of the international response in Sierra Leone (6, 7). To properly evaluate the control efforts, and plan for future outbreaks of EVD, it is therefore crucial to understand how many cases were likely averted as a result of the response.

Mathematical models have been used prospectively to estimate the potential impact of additional beds (8–11). However, evaluating the effect of control measures retrospectively is more challenging,

because a model must disentangle the reduction in transmission due to improved bed capacity from other factors. Behavior changes (12), community engagement, improved case finding, and an increase in safe burials (5) could all have contributed to a reduction in transmission. Indeed, many Ebola facilities were designed to be part of a package of interventions, combining treatment beds with community-based infection control (3).

To estimate how EVD transmission changed as interventions were introduced, we developed a stochastic mathematical model of Ebola transmission in Sierra Leone. The model was stratified by district, and incorporated available data on bed capacity in ETUs, EHCs, and CCCs (13). As beds were not the only control measure in place, we also included a time-varying transmission rate in the model (4, 14) to capture any variation in transmission which was not explained by the introduction of beds.

As not all new cases in Sierra Leone occurred among known contacts of EVD patients (15), we accounted for potential underreporting in our model. In our main analysis, we assumed that 60% of infectious individuals would be ascertained (i.e., would be reported and seek treatment), and that it took an average of 4.5 d for these individuals to be reported (16). We also included the possibility of variability in the accuracy of reporting, with weekly reported cases following a negative binomial distribution. In the model, stochasticity could therefore be generated by both the transmission process and the reporting process. We assumed infectious individuals who were ascertained attended EHCs/CCCs if beds were available (16); the average time between onset and attendance declined over time, based on reported values for Sierra Leone (*SI Appendix*, Fig. S1). Once test results were received, patients were transferred to an available ETU; we

POPULATION
BIOLOGY

Significance

Between June 2014 and February 2015, thousands of Ebola treatment beds were introduced in Sierra Leone, alongside other infection control measures. However, there has been criticism of the timing and focus of this response, and it remains unclear how much it contributed to curbing the 2014–2015 Ebola epidemic. Using a mathematical model, we estimated how many Ebola virus disease cases the response averted in each district of Sierra Leone. We estimated that 56,600 (95% credible interval: 48,300–84,500) Ebola cases were averted in Sierra Leone as a direct result of additional treatment beds. Moreover, the number of cases averted would have been even greater had beds been available 1 month earlier.

Author contributions: A.J.K., A.C., W.J.E., and S. Funk designed research; A.J.K. performed research; R.E.G. contributed new reagents/analytic tools; A.J.K., A.C., S. Flasche, W.J.E., and S. Funk analyzed data; R.E.G. performed data extraction and cleaning; and A.J.K., A.C., S. Flasche, W.J.E., and S. Funk wrote the paper.

The authors declare no conflict of interest.

This article is a PNAS Direct Submission.

Freely available online through the PNAS open access option.

¹To whom correspondence should be addressed. Email: adam.kucharski@lshtm.ac.uk.

This article contains supporting information online at www.pnas.org/lookup/suppl/doi:10.1073/pnas.1508814112/-DCSupplemental.

assumed this took 2 d on average. If no beds were available at any facility, cases remained in the community. The model structure is shown in Fig. 1, and the full set of parameter values in *SI Appendix, Table S1*.

To allow for a time-varying community transmission rate, we used a flexible sigmoid function (14, 17); depending on parameter values, transmission could be constant over time, or increase or decline. Our model structure therefore made it possible to separate the reduction in infection as a result of additional treatment beds and variation resulting from other effects, such as behavior changes and implementation of safe burials.

We used a Bayesian approach to fit the model to weekly EVD confirmed and probable case data reported in each district of Sierra Leone (18, 19), and to estimate how community transmission varied over time. We then used the fitted model to simulate multiple stochastic epidemic trajectories, and measured the number of cases that could have occurred in each district had additional beds not been introduced.

Results

We found that the temporal change in community transmission varied considerably between different regions (Fig. 2). In Bo and Moyamba, for example, the level of community transmission remained relatively flat, whereas in Bombali, Kailahun, Port Loko, and Western Area, a significant decline in community transmission occurred alongside the reduction in transmission resulting from additional beds. In districts where there was greater variation in disease incidence, such as Kambia and Kenema, there was considerable uncertainty in our estimates of the community transmission rate. We found that the decline in community transmission in each of the 12 districts was strongly associated with the initial basic reproduction number, but less so with the total number of cases (*SI Appendix, Table S2*). There was also a geographical structure to the decline, with a greater drop occurring in districts in the north and east of the country (*SI Appendix, Fig. S2*).

To measure how many cases control measures may have averted, we removed all CCC, EHC, and ETU beds introduced during the period of observation and simulated stochastic epidemic trajectories using our estimates for the time-varying level

of community transmission (*SI Appendix, Fig. S3*). In this scenario, transmission reductions from factors other than beds, such as reduced infection as a result of behavior changes, were still included. Any difference in epidemic dynamics between this scenario and the original model was therefore only the result of the removal of treatment beds.

Our results suggest that the increase in beds averted a limited number of cases in districts without ongoing transmission (e.g., Pujehun) but in districts with large outbreaks—such as Bombali and Western Area—there would have been thousands more infections without the introduction of beds. In Kenema, which had highly variable incidence data, there was substantial variation in the background transmission rate, and hence it was not possible to detect a significant effect of interventions; the 95% credible interval (CI) for cases averted includes zero in Table 1. Across all 12 districts, we estimated that 56,600 (95% CI: 48,300–84,500) cases were averted in total between June 2014 and February 2015 as a result of additional beds.

As a sensitivity analysis, we also estimated how many cases would have been averted if 40% or 80% of cases were ascertained, rather than 60% as in our main analysis (*SI Appendix, Tables S3 and S4*). If 80% of cases were ascertained, we estimated that 148,000 (95% CI: 115,000–219,000) cases were potentially averted across all districts as a result of the introduction of beds; when ascertainment was 40%, the additional beds averted 29,200 (95% CI: 24,500–47,700) cases. In our main analysis, we also assumed an infectious period of 10.9 d, based on reported time from onset-to-death, and onset-to-hospital discharge (details in *SI Appendix*). As some cases may have ceased to be infectious before discharge, as a sensitivity analysis we refit the model with a 9-d infectious period, equal to the average time of infectiousness for fatal cases. Our results did not change substantially under this assumption (*SI Appendix, Table S5*).

In the model, we also assumed that transmission in each district was independent of the others. In reality, however, infectious individuals occasionally traveled between different areas (20). To assess how this could affect our estimates of cases averted, we resimulated outbreaks using the fitted model, but with additional infectious individuals introduced at a rate of either one per day or one per week in each district. When there was an average of one additional infection introduced per week, our estimates increased slightly (*SI Appendix, Table S6*); when one additional infection was introduced per day, the increase was larger, with an estimated 72,900 (95% CI: 61,700–87,900) cases averted across the country.

As well as measuring the effect of actual control measures, we were also able to estimate what impact the introduction of beds would have had earlier in the epidemic. Using the fitted model, we simulated epidemic trajectories under the assumption that the same numbers of beds were introduced 4 wk earlier than in reality (*SI Appendix, Fig. S4*). In this scenario, we estimated 69,100 (95% CI: 59,500–122,000) cases would have been averted, which is 12,500 higher than the number we estimated were actually averted (Table 1).

Discussion

Using a district-level mathematical model of EVD transmission, we have examined the effect of control measures on epidemic dynamics in Sierra Leone. In particular, we estimated the effect of the reduction in community transmission and additional treatment beds on the number of EVD cases. We found considerable geographic variation: in some districts, there was a noticeable shift in epidemic dynamics as a result of changes in community transmission and increased bed capacity; in other areas, the impact of control measures was less clear.

Although we could measure the number of beds available over time, there were some additional components of the treatment process that were less well known. We used reported data on time to hospital admission in Sierra Leone to parameterize our model

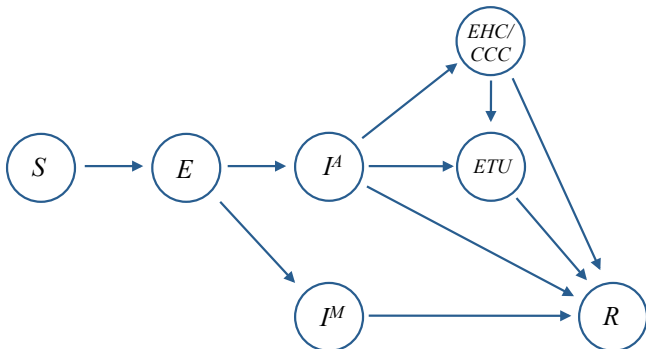


Fig. 1. Model structure. Individuals start off susceptible to infection (S). Upon infection with Ebola they enter an incubation period (E), then at symptom onset they become infectious; these individuals either eventually become ascertained (I^A) or do not (I^M). Individuals who are ascertained initially seek health care in EHCs/CCCs (or ETUs if these are full); if no beds are available, they remain infectious in the community until the infection is resolved (R), i.e., they have recovered, or are dead and buried. Patients in EHC/CCCs are transferred to ETUs once they have been tested for Ebola, which takes an average of 2 d. Patients remain in ETUs until the infection is resolved. We assume the latent period is 9.4 d, the average time from onset to EHC/CCC attendance declines from an initial value of 4.6 d (*SI Appendix, Fig. S1*), and individuals who do not seek treatment are infectious for 10.9 d on average (details in *SI Appendix*).

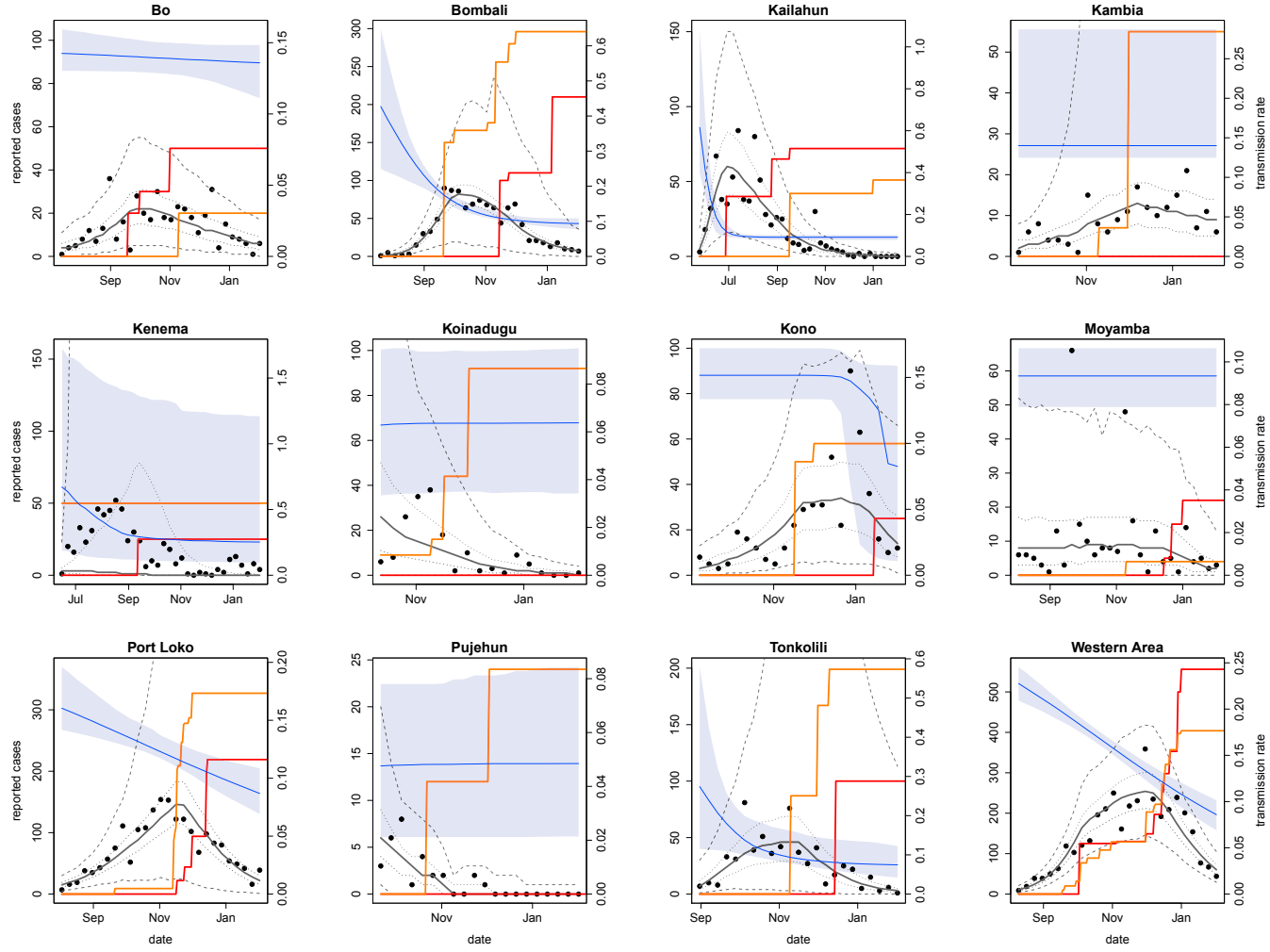


Fig. 2. Community transmission and bed capacity in Sierra Leone over time. Blue lines show estimated median community transmission rate, shaded area shows 95% CI (right-hand axis). Black dots show weekly reported confirmed and probable cases in each district up to February 2, 2015 (left-hand axis). Gray lines show median number of cases generated from 1,000 simulations of the fitted model, with 50% CI given by dotted gray lines and 95% CI given by dashed lines. Solid red lines, ETU bed capacity; orange lines, EHC/CCC bed capacity.

(1, 16), but this may have varied between districts. We also assumed that individual infectiousness remained constant throughout the symptomatic period. If most transmission occurs in the later stages of infection, as viral load data might suggest (21), treatment beds could have had a greater impact on transmission reduction by isolating cases at their most infectious. This would make our estimate for cases averted as a result of additional beds conservative.

In the model, patients also sought treatment within their home district. However, in the early stages of the epidemic, several cases admitted to the ETU in Kailahun were from outside the district (20). This may have increased the benefits of bed introduction, by reducing transmission in locations without treatment beds; it may also have impeded control efforts, by making contact tracing and safe burials more difficult (20). In addition, faster turnaround time in laboratory testing may have reduced the time spent in EHCs/CCCs before moving to ETUs (Sierra Leone Ebola labs project – beating the outbreak at source; <https://publichealthmatters.blog.gov.uk/2015/03/18/sierra-leone-ebola-labs-project-beating-the-outbreak-at-source/>), and led to more EHC beds becoming available per day. Although there were occasional details of the number of patients in isolation in different districts in Ministry of Health and Sanitation situation reports (15), overall these data were incomplete. If more complete EHC/CCC/ETU data were

available, it would be possible to validate our model estimates for the number of cases hospitalized over time.

Our results also emphasize the highly variable nature of Ebola transmission. Even in retrospect, it was difficult to measure the effect of changes in transmission and additional beds on the number of EVD cases in some areas. It is also likely that the introduction of Ebola facilities helped stimulate other infection control measures, including safe burials and improved contact tracing (3). In our simulated scenarios, we removed only treatment beds; in practice, a lack of treatment centers would also likely have led to fewer safe burials, and hindered investigation of cases' contacts. With better data on the timing and role of different interventions—both clinical and nonclinical—it would be possible to obtain more accurate estimates about the precise contribution of different factors to the dynamics of EVD in Sierra Leone. In particular, it is important to understand how awareness of EVD influences behavior during an outbreak (22), and how this change in behavior might affect disease dynamics (23, 24).

In the absence of such data, we concentrated on the impact of additional treatment beds alone; we assumed the level of community transmission declined regardless of the number of beds. An alternative approach would be to assume that transmission would remain at the same level as was in the early phase of the

Table 1. Estimated number of cases averted up to February 2, 2015 as a result of additional treatment beds

District	Initial R_0	Beds introduced	Additional beds	Beds 4 wk earlier
Bo	1.6 (1.4–1.7)	124	6,310 (4,150–9,040)	6,820 (4,730–9,620)
Bombali	5.2 (2.9–7.9)	506	6,480 (1,800–22,900)	7,630 (2,320–34,500)
Kailahun	8.4 (5.3–16.2)	123	3,650 (2,250–6,750)	4,580 (3,290–7,460)
Kambia	1.5 (1.4–3.6)	55	545 (2–4,430)	748 (4–15,400)
Kenema	7.4 (2.1–19.4)	75	1 (0–10,500)	3 (0–23,800)
Koinadugu	0.7 (0.3–1.1)	92	35 (11–104)	97 (48–206)
Kono	1.6 (1.4–1.9)	83	1,570 (928–2,430)	2,060 (1,490–3,060)
Moyamba	1 (0.9–1.2)	34	130 (77–197)	237 (145–366)
Port Loko	1.8 (1.6–2.2)	546	3,850 (853–13,400)	5,660 (1,180–26,900)
Pujehun	0.5 (0.2–1.2)	24	11 (2–34)	22 (6–55)
Tonkolili	3.5 (1.3–8.4)	349	568 (140–2,900)	959 (272–5,940)
Western Area	2.5 (2.2–2.8)	960	32,600 (25,500–40,200)	39,200 (32,100–47,100)
Total		2,971	56,600 (48,300–84,500)	69,100 (59,500–122,000)

For each district, we estimated the median number of additional cases that would result in the original fitted model, with community transmission rate varying as shown in Fig. 2. We then considered two scenarios: additional EHC/CCC/ETU beds introduced as in reality, and the same additional beds introduced 4 wk earlier, and estimated the number of cases averted in each scenario (95% CI in parentheses). The median posterior estimates for initial R_0 (95% CI in parentheses) and total numbers of additional EHC/CCC/ETU beds introduced in each district are shown for comparison.

epidemic (9, 10). As our estimate of the basic reproduction number R_0 was above 1 in most districts initially (Table 1), epidemic theory suggests the outbreak would have continued to grow exponentially in these regions under the assumption of no change in transmission, until there were insufficient susceptible individuals for the infection to persist. The corresponding number of cases averted would therefore have been extremely large. However, it was not clear that R_0 would have remained unchanged for such a long period. Evidence from past EVD epidemics indicates that changes in behavior can reduce transmission independently of external interventions (22, 25).

Even under our conservative assumption that the introduction of EHCs/CCCs/ETUs reduced transmission only by isolating more patients, we estimated that around 57,000 cases were averted in Sierra Leone as a result of additional treatment beds. Given that the case fatality rate of Ebola in Sierra Leone is near 70% (16), this suggests that the scale-up of local and international efforts to combat the epidemic is likely to have averted over 40,000 Ebola deaths in the country between June 2014 and February 2015. Moreover, the reduction in Ebola transmission will also have halted the damaging secondary effects of the epidemic, including the suspension of access to maternal health and vaccination programs (26, 27).

Materials and Methods

Transmission Model. To model the effect of treatment beds on Ebola transmission, we used a susceptible-exposed-infectious-removed (SEIR) framework that incorporated ETUs and EHCs/CCCs (8). We used a relatively simple framework as we were fitting to only a single case timeseries for each district (14). In the model, individuals started off susceptible to infection (5). Upon infection with Ebola they entered an incubation period (E), then at symptom onset they became infectious. As there is evidence that not all Ebola cases have been reported (1), we assumed that only a proportion r of newly infectious individuals would eventually be ascertained and seek treatment. This category was denoted I^A . The other proportion $1-r$ would not be ascertained; this group was denoted I^M . We assumed that it took an average of $1/\tau_I$ d for ascertained cases to be reported to the Ministry of Health. After becoming symptomatic in the model, cases in I^A sought health care in EHCs/CCCs (H). They took an average of $1/\tau_H$ d to attend these centers. If no EHC/CCC beds were available, the patient would attend an ETU. If no ETU bed were available, the patient remained infectious in the community until the infection was resolved (R); i.e., they had recovered, or were dead and buried. Once in an EHC/CCC, patients were tested for Ebola (we assumed this took an average of 2 d) then progressed to an ETU if a bed was available. Patients stayed for an average of $1/\tau_D$ d in an ETU before the

disease was resolved (either through recovery or death). The probability that Ebola-positive individuals were admitted to an EHC/CCC, p_H , when they attended the center depended on whether the center was full or not. We assumed that some patients attending EHCs/CCCs were Ebola-negative, which had the effect of reducing the available bed capacity by a factor α . The probability that Ebola-positive individuals were admitted to an EHC/CCC upon attendance was therefore

$$p_H = \begin{cases} 1 & \text{if } \alpha B_H > H \\ 0 & \text{if } \alpha B_H = H \end{cases} \quad [1]$$

where B_H denotes the total capacity of the EHCs/CCCs. Likewise, the probability that individuals were admitted/transferred to an ETU was

$$p_U = \begin{cases} 1 & \text{if } B_U > U \\ 0 & \text{if } B_U = U \end{cases} \quad [2]$$

where B_U denotes the capacity of the ETUs. We assumed that the population was initially fully susceptible to infection. We assumed the average latent period $1/\nu$ was 9.4 d, and the average duration of infectiousness in the community $1/\gamma$ to be 10.9 d in our main analysis; as a sensitivity analysis we also considered an infectious period of 9 d. The average time from onset-to-outcome for individuals that seek treatment was assumed to be 11.3 d (details in *SI Appendix*).

We obtained EHC/CCC/ETU opening dates from the Humanitarian Data Exchange (13), and cleaned ambiguous or missing dates using reports from the World Health Organization (WHO), Médecins Sans Frontières, UNICEF, and other partners. If the precise date of opening or change in capacity was not known, we used the first date for which we could find confirmation of the center being open with a given capacity. This could have made our analysis more conservative, as some centers may in reality have opened earlier than we presumed. One field study in Bo estimated that 54% of EVD cases made it into the district-level situation reports (28); in turn, the numbers of cases in these reports are typically slightly lower than the numbers in the final WHO patient database (1). Therefore, we made the assumption that 60% of symptomatic cases were ascertained in our main analysis (4), and considered 40% and 80% ascertainment as a sensitivity analysis. We assumed that it took an average of 4.5 d for these cases to be reported after symptom onset (16). In the model, the time between onset and attendance of EHCs/CCCs declined from 4.6 to 1.3 d between July 2014 and April 2015 (*SI Appendix*, Fig. S1); the average duration spent in EHC/CCC before moving to an ETU was 2 d; and the average time spent in an ETU was initially $11.3 - 4.6 - 2 = 4.7$ d. We assumed that 50% of beds in EHCs/CCCs were occupied by Ebola-negative patients (15) (i.e., $\alpha = 0.5$). We also allowed community transmission to potentially vary over time by modeling the transmission rate at time t , β_t , as a sigmoid (14, 17):

$$\beta_t = \hat{\beta} \left(1 - \frac{a_2}{1 + e^{-a_1(t-a_c)}} \right), \quad [3]$$

where $\hat{\beta}$, a_1 , a_2 , and a_c were parameters to be fitted. We modeled transmission dynamics using a stochastic model, with environmental noise acting on the transmission rate (29):

$$dS_t = -\beta_t \xi_t \frac{S_t (I_t^A + I_t^M)}{N} dt, \quad [4]$$

$$dE_t = \beta_t \xi_t \frac{S_t (I_t^A + I_t^M)}{N} dt - \nu E_t dt, \quad [5]$$

$$dI_t^A = \nu E_t dt - p_H \tau_H I_t^A dt - (1-p_H)(1-p_U)\gamma I_t^A dt \\ - (1-p_H)p_U \tau_H I_t^A dt, \quad [6]$$

$$dI_t^M = (1-\nu) \nu E_t dt - \gamma I_t^M dt, \quad [7]$$

$$dH_t = p_H \tau_H I_t^A dt - p_U \tau_U H_t dt - (1-p_U)\tau_F H_t dt, \quad [8]$$

$$dU_t = (1-p_H)p_U \tau_H I_t^A dt + p_U \tau_U H_t dt - \tau_D U_t dt, \quad [9]$$

$$dR_t = \gamma I_t^M dt + \tau_D U_t dt + (1-p_H)(1-p_U)\gamma I_t^A dt \\ + (1-p_U)\tau_F H_t dt, \quad [10]$$

$$dX_t = \nu \tau_F E_t dt. \quad [11]$$

$$[12]$$

$$[13]$$

Here N is the total population size, X_t is the cumulative total of ascertained Ebola cases, β_t is the rate of transmission at time t , and ξ_t is a lognormal (and hence positive) noise term with mean 1 and variance σ^2 :

$$\log(\xi_t) dt = \sigma dW - \frac{\sigma^2}{2} dt, \quad [14]$$

where W is Brownian motion (29). Model structure and parameters are shown in *SI Appendix*, Fig. S6. The model was simulated using the Euler–Maruyama method with intervals of $dt=1/10$ d. Population size N for each district was taken from Sierra Leone census data (30).

Model Fitting. We fitted the model to weekly incidence data (i.e., number of new confirmed and probable cases per week) from Sierra Leone reported in the WHO patient database (1). As described in a previous study, we also used data from the Sierra Leone Ministry of Health (15) when more recent case data were not available in the WHO database (4). We excluded Bonthe district from the analysis as there were small numbers of confirmed or probable cases, which were spaced several weeks apart. It is therefore unlikely there was sustained transmission in this area. For each of the other districts, we used the first reported week of sustained transmission (i.e.,

there were cases in that week and the following week) as the first data point in the time series. The last data point for all districts was February 2, 2015, as the number of cases had declined to minimal levels in most areas by this point. In the model, incidence in week t , denoted x_t , was given by the difference in cumulative reported cases over the previous 7 d, i.e., $x_t = X(t) - X(t-7)$. As situation reports were only issued on w out of 7 d in some weeks, we scaled these weeks by a factor $\kappa_t = w/7$. We also included the possibility of variability in the accuracy of reporting in the situation reports. We assumed the number of reported cases in week t followed a negative binomial distribution with mean $x_t \kappa_t$ and variance $x_t \kappa_t + \phi^2 \kappa_t^2 x_t^2$ (4).

Model fitting was performed using a particle Markov chain Monte Carlo (MCMC) algorithm (19) with an adaptive multivariate normal proposal distribution (31). For each district, we fitted the initial number of infective individuals (including both ascertained and missed) at the start of the outbreak, $I_0 = I(0)$; the volatility of the transmission rate, σ ; over-dispersion of reporting, ϕ ; the initial transmission rate $\hat{\beta}$; and the two shape parameters for the transmission rate sigmoid, a_1 , a_2 , and a_c . We used uniform positive priors for all parameters, with the exception of a_2 , which we constrained to the interval $(-\infty, 1)$ by imposing reflective boundary conditions during parameter resampling. Posterior estimates for $R_0 = \beta_0/\gamma$, I_0 , σ , ϕ , and the 4 sigmoid parameters (taken from 50,000 MCMC iterations, following a burn-in period of 10,000 iterations) are given in *SI Appendix*, Figs. S6–S17; the posterior distribution of the sigmoid is shown in Fig. 2 (blue line and shaded region). The model was implemented in R Version 3.1.3, and parallelized for multiple districts using the doMC library (32, 33).

Estimating Cases Averted. To estimate the number of infections averted as a result of control measures, we first estimated the total number of infections (i.e., the cumulative number of individuals who leave the S compartment) up to February 2, 2015 using the posterior parameter estimates from our fitted model. We define this as the “baseline scenario.” Next, we assumed that the community transmission rate varied as in the baseline scenario, but no additional EHCs/CCCs/ETUs were introduced. This was equivalent to assuming that changes aside from bed introductions—such as shifts in behavior, increased number of safe burials, improved infection control—would have happened regardless of whether additional beds were made available. We ran 1,000 bootstrap simulations under this scenario, and compared the total number of infections with the baseline scenario. In our main analysis, we assumed that 60% of cases were ascertained (i.e., $r = 0.6$). To test how sensitive our results were to this assumption, we also refitted the model to each district with $r = 0.4$ and 0.8, and used these fitted models to estimate the number of cases averted in the two different scenarios above. The results are given in *SI Appendix*, Tables S3 and S4.

ACKNOWLEDGMENTS. This work was funded by the Research for Health in Humanitarian Crises (R2HC) Programme, managed by Research for Humanitarian Assistance (Grant 13165). A.J.K. acknowledges support from the Research and Policy for Infectious Disease Dynamics (RAPIDD) program of the Science & Technology Directorate, Department of Homeland Security, and the Fogarty International Center, National Institutes of Health.

1. World Health Organization (2015) Ebola response roadmap situation reports. Available at apps.who.int/ebola/en/current-situation/ebola-situation-report-20-may-2015. Accessed July 1, 2015.
2. Whitty CJ, et al. (2014) Infectious disease: Tough choices to reduce Ebola transmission. *Nature* 515(7526):192–194.
3. World Health Organization (2014) Key considerations for the implementation of Community Care Centres. WHO Report. Available at apps.who.int/iris/bitstream/10665/146469/1/WHO_EVD_Guidance_Strategy_14.3_eng.pdf. Accessed December 10, 2014.
4. Camacho A, et al. (2015) Temporal changes in Ebola transmission in Sierra Leone and implications for control requirements: A real-time modelling study. *PLoS Curr* 7:PMC4339317.
5. Nielsen CF, et al.; Centers for Disease Control and Prevention (2015) Improving burial practices and cemetery management during an Ebola virus disease epidemic - Sierra Leone, 2014. *MMWR Morb Mortal Wkly Rep* 64(1):20–27.
6. Gulland A (2014) UK's plan to build community care centres for Ebola patients is questioned. *BMJ* 349:g6788.
7. BBC News (2015) Ebola crisis: Government response “far too slow.” Available at www.bbc.co.uk/news/uk-31366626. Accessed March 15, 2015.
8. Kucharski AJ, et al. (2015) Evaluation of the benefits and risks of introducing Ebola community care centers, Sierra Leone. *Emerg Infect Dis* 21(3):393–399.
9. Lewnard JA, et al. (2014) Dynamics and control of Ebola virus transmission in Montserrat, Liberia: A mathematical modelling analysis. *Lancet Infect Dis* 14(12):1189–1195.
10. Meltzer MI, et al. (2014) Estimating the future number of cases in the Ebola epidemic – Liberia and Sierra Leone, 2014–2015. *MMWR Morb Mortal Wkly Rep* 63(3):1–14.
11. Merler S, et al. (2015) Spatiotemporal spread of the 2014 outbreak of Ebola virus disease in Liberia and the effectiveness of non-pharmaceutical interventions: A computational modelling analysis. *Lancet Infect Dis* 15(2):204–211.
12. Funk S, Knight GM, Jansen VA (2014) Ebola: The power of behaviour change. *Nature* 515(7528):492.
13. The Humanitarian Data Exchange (HDX) (2014) West Africa: Ebola Outbreak. Available at data.hdx.rwlabs.org. Accessed March 27, 2015.
14. Camacho A, et al. (2014) Potential for large outbreaks of Ebola virus disease. *Epidemics* 9:70–78.
15. Sierra Leone Ministry of Health and Sanitation (2014) Ebola virus disease - situation report. Available at health.gov.sl/?page_id=583. Accessed March 20, 2015.
16. WHO Ebola Response Team (2014) Ebola virus disease in West Africa—the first 9 months of the epidemic and forward projections. *N Engl J Med* 371(16):1481–1495.
17. Chowell G, Hengartner NW, Castillo-Chavez C, Fenimore PW, Hyman JM (2004) The basic reproductive number of Ebola and the effects of public health measures: The cases of Congo and Uganda. *J Theor Biol* 229(1):119–126.
18. King AA, Domenech de Cellès M, Maigpanay FM, Rohani P (2015) Avoidable errors in the modelling of outbreaks of emerging pathogens, with special reference to Ebola. *Proc Biol Sci* 282(1806):20150347.
19. Andrieu C, Doucet A, Holenstein R (2010) Particle Markov chain Monte Carlo methods. *J R Stat Soc Series B Stat Methodol* 72(3):269–342.
20. Dallatomasina S, et al. (2015) Ebola outbreak in rural West Africa: Epidemiology, clinical features and outcomes. *Trop Med Int Health* 20(4):448–454.
21. Towner JS, et al. (2004) Rapid diagnosis of Ebola hemorrhagic fever by reverse transcription-PCR in an outbreak setting and assessment of patient viral load as a predictor of outcome. *J Virol* 78(8):4330–4341.

22. Hewlett BS, Amola RP (2003) Cultural contexts of Ebola in northern Uganda. *Emerg Infect Dis* 9(10):1242–1248.
23. Ferguson N (2007) Capturing human behaviour. *Nature* 446(7137):733.
24. Funk S, Gilad E, Watkins C, Jansen VA (2009) The spread of awareness and its impact on epidemic outbreaks. *Proc Natl Acad Sci USA* 106(16):6872–6877.
25. Breman J, et al. (1978) The epidemiology of Ebola hemorrhagic fever in Zaire, 1976. *Ebola Virus Haemorrhagic Fever*, ed Pattyn SR (Elsevier, Amsterdam), pp 85–97.
26. Hayden EC (2015) Maternal health: Ebola's lasting legacy. *Nature* 519(7541): 24–26.
27. Takahashi S, et al. (2015) Reduced vaccination and the risk of measles and other childhood infections post-Ebola. *Science* 347(6227):1240–1242.
28. Roberts L (2014) Day 54: Surveillance at odds with justice and the little people. Available at pfmhcolumbia.wordpress.com. Accessed January 5, 2015.
29. Ionides EL, Bretó C, King AA (2006) Inference for nonlinear dynamical systems. *Proc Natl Acad Sci USA* 103(49):18438–18443.
30. National Statistics of Sierra Leone (2004) 2004 population and housing census. Available at www.sierra-leone.org/Census/ssl_final_results.pdf. Accessed April 17, 2015.
31. Roberts GO, Rosenthal JS (2009) Examples of adaptive MCMC. *J Comput Graph Stat* 18:349–367.
32. Revolution Analytics (2014) doMC package. Available at cran.r-project.org/web/packages/doMC/index.html. Accessed March 15, 2015.
33. R Development Core Team (2015) The R Project for Statistical Computing. Available at www.r-project.org/. Accessed March 15, 2015.

Supplementary materials: Measuring the impact of Ebola control measures in Sierra Leone

Adam J. Kucharski¹, Anton Camacho¹, Stefan Flasche¹, Rebecca E. Glover¹, W. John Edmunds¹, Sebastian Funk¹

¹ Centre for the Mathematical Modelling of Infectious Diseases, Department of Infectious Disease Epidemiology, London School of Hygiene & Tropical Medicine

S1 Estimation of duration of infectiousness

The duration of infectiousness, $1/\gamma$, was first calculated separately for cases that result in death and recovery. For cases that resulted in death, the duration of infectiousness was calculated as the reported average duration from onset-to-death (8.6 days) [1] plus one day for burial for cases that were not ascertained ($1-r$) [2]. For cases that recovered, we used the duration from onset-to-hospital discharge (17.2 days) [1] minus 48 hours, as this is the time that would have elapsed since first possible confirmation that the patient was no longer infectious (to be discharged, a patient must test negative for Ebola twice, with an interval of 48 hours between tests [3]). We then combined the two estimates, weighting by the case fatality rate (69%) [1]:

$$1/\gamma = 0.69 \times (8.6 + (1 - r)) + (1 - 0.69) \times (17.2 - 2) \quad (\text{S1})$$

In our main analysis 60% of cases were ascertained, and hence $1/\gamma=10.9$ days. As a sensitivity analysis we also considered an infectious period of 9 days, equal to the reported average duration from onset-to-death (8.6 days) plus one day for burial for cases that were not ascertained (under 60% ascertainment).

By a similar calculation, the average from onset-to-outcome for cases that seek treatment was $0.69 \times 8.6 + (1 - 0.69) \times (17.2) = 11.3$ days. This value was used to estimate average duration of stay in EHC/CCC/ETU (Table S1).

References

- [1] WHO Ebola Response Team (2014) Ebola virus disease in West Africa — the first 9 months of the epidemic and forward projections. *New England Journal of Medicine* 371:1481–1495.
- [2] Nielsen CF, et al. (2015) Improving Burial Practices and Cemetery Management During an Ebola Virus Disease Epidemic. Sierra Leone, 2014. *MMWR: Morbidity and mortality weekly report* 64:20–27.
- [3] World Health Organisation (2015) Criteria for declaring the end of the Ebola outbreak in Guinea, Liberia or Sierra Leone. <http://www.who.int/csr/diseases/ebola/declaration-ebola-end/en/>.
- [4] Breman J, et al. (1978) The epidemiology of Ebola hemorrhagic fever in Zaire, 1976. *Ebola virus haemorrhagic fever* (Puttn, SR ed), pp 85–97.
- [5] Bentley N (2015) Sierra Leone Ebola labs project – beating the outbreak at source. *Public Health England Blog*.
- [6] World Health Organisation (2015) Ebola response roadmap situation reports. apps.who.int/ebola/en/current-situation/ebola-situation-report-20-may-2015.

Supplementary Tables

Table S1 : Parameter definitions and values.

Parameter	Definition	Value	Reference
$1/\nu$	Latent period	9.4 days	[1, 4]
$1/\gamma$	Mean duration of infectiousness	10.9 days	See supplementary text
$1/\tau_H$	Mean time from onset of symptoms to EHIC/CCC admission	1.8 to 4.6 days	See Fig. S1
$1/\tau_U$	Mean time spent in EHIC/CCC awaiting test results	2 days	[5]
$1/\tau_D$	Mean duration of stay in ETU	$11.3 - 1/\tau_H - 1/\tau_U$	
$1/\tau_F$	Mean duration of stay in EHIC/CCC if no ETU beds	$11.3 - 1/\tau_H$	
r	Mean time from onset of symptoms to case report	4.5 days	[1]
ρ	Proportion of cases that are ascertained	0.4, 0.6, 0.8	[1]
β	Initial transmission rate	Estimated	
a_1	Slope of change in transmission rate	Estimated	
a_2	Final value of transmission rate	Estimated	
a_{τ}	Midpoint of time of change in transmission rate	Estimated	
σ	Variability of transmission rate	Estimated	
ϕ	Overdispersion of reporting process	Estimated	

Table S2: Relationship between relative reduction in R_0 , initial R_0 , and total cases per 100,000 population in each district. Relative reduction in R_0 is calculated as $1 - R_0^T/R_0^0$, where R_0^0 is the median basic reproduction number at the start of the period of study, and R_0^T is the median basic reproduction number on 2nd February 2015. Association between reduction and the other two variables was tested using Pearson's product moment correlation coefficient.

District	Relative reduction in R_0	Initial R_0	Cases/100,000
Pujehun	-8.74E-11	0.546	12.7
Koinadugu	-2.52E-15	0.792	62.1
Bo	1.52E-08	1.76	89.7
Kambia	0.000795	1.98	69.1
Tonkolili	0.00158	1.31	179
Moyamba	0.00281	1.1	107
Port Loko	0.0661	1.55	437
Kono	0.148	1.81	151
Kenema	0.299	2.39	114
Western Area	0.378	2.41	395
Bombali	0.553	3.36	264
Kailahun	0.604	3.31	206
Correlation:	0.905	0.445	
P-value:	<0.0001	0.147	

Table S3: Estimated number of cases averted up to 2nd February 2015 as a result of additional treatment beds, when $1/\gamma=10.9$ days and 80% cases are ascertained.

District	Initial R_0	Beds introduced	Additional beds	Beds 4 weeks earlier
Bo	1.8 (1.6-2.3)	124	14,600 (388-39,400)	15,100 (423-489,700)
Bombali	3.4 (2.2-5.2)	506	8,570 (4-73,400)	12,500 (2-207,000)
Kailahun	3.3 (2.9-3.8)	123	20,500 (12,200-36,900)	21,400 (13,200-37,700)
Kambia	2.0 (1.4-9.6)	55	532 (0-4,970)	679 (0-20,000)
Kenema	2.4 (1.7-4.0)	75	274 (199-411)	440 (304-635)
Koinadugu	0.8 (0.6-1.2)	92	62 (26-189)	144 (79-290)
Kono	1.8 (1.5-16.2)	83	1,730 (0-3,580)	2,440 (0-7,810)
Moyamba	1.1 (0.9-5.4)	34	138 (72-253)	243 (153-442)
Port Loko	1.6 (1.5-1.7)	546	8,410 (5,680-11,600)	10,300 (7,160-14,200)
Pujehun	0.5 (0.4-1.0)	24	12 (5-41)	25 (12-58)
Tonkolili	1.3 (1.1-2.8)	349	1,300 (10-8,470)	1,680 (18-12,000)
Western Area	2.4 (2.3-2.6)	960	82,800 (67,100-109,000)	89,200 (73,300-114,000)
Total		2971	148,000 (115,000-219,000)	159,000 (126,000-351,000)

Table S4: Estimated number of cases averted up to 2nd February 2015 as a result of reduction in community transmission and/or additional treatment beds, when $1/\gamma=10.9$ days and 40% cases are ascertained.

District	Initial R_0	Beds introduced	Additional beds	Beds 4 weeks earlier
Bo	1.9 (1.4-3.2)	124	2,150 (1,140-4,670)	2,770 (1,430-8,380)
Bombali	4.1 (3.3-5.7)	506	3,460 (2,960-4,270)	4,600 (4,000-5,700)
Kailahun	6.2 (1.7-11.5)	123	1,420 (0-9,520)	2,430 (1-22,800)
Kambia	1.4 (1.2-1.5)	55	432 (295-578)	641 (446-816)
Kenema	2.2 (1-14.7)	75	120 (0-12,700)	181 (0-18,400)
Koinadugu	0.6 (0.3-0.9)	92	29 (12-96)	95 (51-208)
Kono	3.5 (1.3-19.3)	83	78 (0-3,020)	132 (0-8,600)
Moyamba	1.1 (0.8-12.2)	34	97 (0-549)	187 (0-1,340)
Port Loko	2.3 (1.8-3.0)	546	2,450 (369-6,980)	4,230 (629-12,600)
Pujehun	0.5 (0.3-1.4)	24	9 (2-28)	23 (9-51)
Tonkolili	2.9 (1.7-6.6)	349	400 (133-850)	788 (292-1,660)
Western Area	2.5 (2.3-2.9)	960	17,600 (14,600-20,900)	25,000 (19,800-28,700)
Total		2971	29,200 (24,500-47,700)	42,600 (34,700-75,000)

Table S5: Estimated number of cases averted up to 2nd February 2015 as a result of additional treatment beds, when $1/\gamma=9$ days and 60% cases are ascertained.

District	Initial R_0	Beds introduced	Additional beds	Beds 4 weeks earlier
Bo	1.6 (1.4-2)	124	5,170 (2,710-8,920)	5,700 (3,270-9,460)
Bombali	5.7 (3.8-8.2)	506	5,640 (4,720-6,900)	6,720 (5,800-7,940)
Kailahun	6 (4.1-14.8)	123	3,550 (1,830-5,880)	4,330 (2,940-6,770)
Kambia	1.5 (1.2-3)	55	547 (89-5,700)	745 (152-6,900)
Kenema	3.5 (1.4-14.4)	75	0 (0-31,300)	1 (0-47,700)
Koinadugu	0.7 (0.4-2.3)	92	31 (9-121)	95 (42-222)
Kono	1.6 (1.1-12)	83	1,180 (0-4,220)	1,640 (0-12,700)
Moyamba	1.1 (0.7-6.6)	34	121 (0-1,380)	224 (0-2,590)
Port Loko	1.7 (1.4-2)	546	3,960 (3,250-5,080)	5,760 (4,960-7,120)
Pujehun	0.6 (0.3-0.8)	24	10 (2-27)	21 (8-47)
Tonkolili	2.8 (1.4-6.8)	349	571 (370-846)	956 (689-1,290)
Western Area	2.3 (2.1-2.6)	960	33,100 (26,200-41,200)	39,500 (32,500-47,200)
Total		2971	54,800 (45,400-75,100)	67,500 (58,500-118,000)

Table S6: Estimated number of cases averted up to 2nd February 2015 as a result of additional treatment beds, when districts have additional imported cases. These extra cases are added to the I_t^A and I_t^N compartments in the model (weighted by the ascertainment rate, r) at an average rate of either one per day or one per week. We assume $1/\gamma=10.9$ days and 60% cases are ascertained.

District	Initial R_0	Beds introduced	With one imported case per day	With one imported case per week
Bo	1.6 (1.4–1.7)	124	8,450 (5,600–13,100)	6,680 (4,320–10,500)
Bombali	5.2 (2.9–7.9)	506	14,300 (3,850–18,400)	10,500 (1,090–16,100)
Kailahun	8.4 (5.3–16.2)	123	5,070 (2,900–9,190)	3,960 (2,190–7,090)
Kambia	1.5 (1.4–3.6)	55	936 (13–3,260)	612 (13–4,180)
Kenema	7.4 (2.1–19.4)	75	2 (0–12,700)	1 (0–16,200)
Koinadugu	0.7 (0.3–1.1)	92	49 (19–170)	39 (14–114)
Kono	1.6 (1.4–1.9)	83	1,930 (1,030–2,980)	1,610 (941–2,480)
Moyamba	1 (0.9–1.2)	34	125 (89–231)	125 (77–205)
Port Loko	1.8 (1.6–2.2)	546	4,210 (1,280–9,380)	3,900 (1,060–15,300)
Pujehun	0.5 (0.2–1.2)	24	19 (3–46)	11 (3–43)
Tonkolili	3.5 (1.3–8.4)	349	780 (61–2,710)	601 (28–4,610)
Western Area	2.5 (2.2–2.8)	960	35,600 (27,600–46,500)	33,100 (25,300–42,300)
Total		2971	72,900 (61,700–87,900)	64,900 (49,800–93,100)

Supplementary Figures

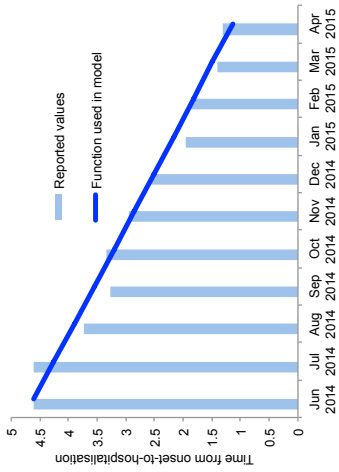


Figure S1: Decline in time from onset-to-isolation. We assume the delay in June and July 2014 was equal to the average value reported in an early summary analysis [1]; the remaining values come from WHO situation reports [6]. We used linear regression to obtain the continuous-time function used in the model.

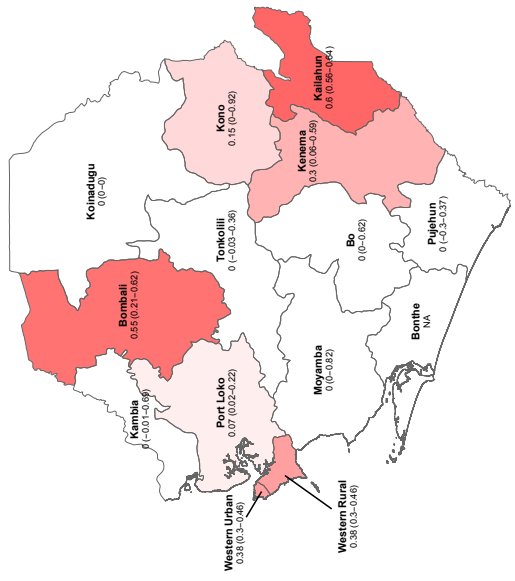


Figure S2: Relative reduction in R_0 in different districts. This is calculated as $1 - \frac{R_0^T}{R_0^0}$, where R_0^0 is the basic reproduction number at the start of the period of study, and R_0^T is the basic reproduction number on 2nd February 2015. Districts are coloured by median reduction in R_0 , the value for which is given below the district name (95% credible intervals are in parentheses). In the model we treated the two parts of Western Area (Urban and Rural) as one district, as this is how case data were typically reported. There was no estimate of reduction in Bonthe, as we did not fit the model to this district (see main text for details). District boundaries obtained from the GADM database of Global Administrative Areas, freely available from <http://www.gadm.org>.

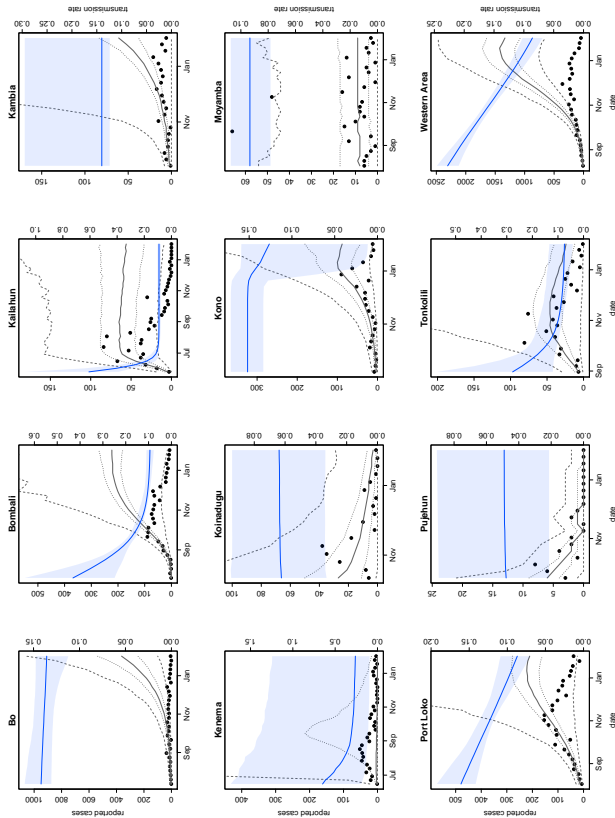


Figure S3: District-level epidemic dynamics in the absence of treatment beds. Gray line shows median number of cases generated from 1000 simulations of the fitted model, with 50% credible intervals given by dotted gray lines and 95% CI given by dashed lines. Blue line shows median community transmission rate, shaded area shows 95% credible interval (right hand axis). Black dots show weekly reported confirmed and probable cases in each district up to 2nd February 2015 (left hand axis).

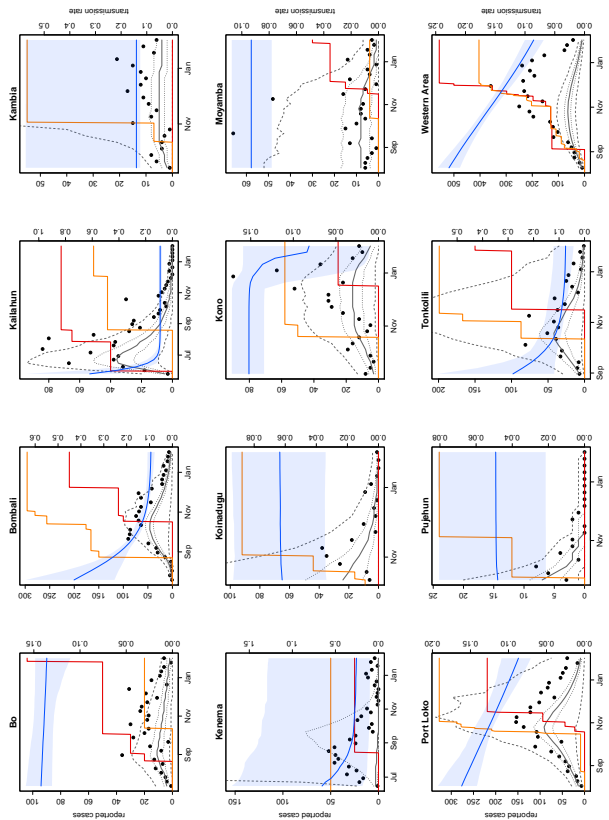


Figure S4: District-level epidemic dynamics when beds are introduced 4 weeks earlier. Gray line shows median number of cases generated from 1000 simulations of the fitted model, with 50% credible intervals given by dotted gray lines and 95% CI given by dashed lines. Blue line shows median community transmission rate, shaded area shows 95% credible interval (right hand axis). Black dots show weekly reported confirmed and probable cases in each district up to 2nd February 2015 (left hand axis). Solid red line, ETU bed capacity; orange line, EHC/CCC bed capacity.

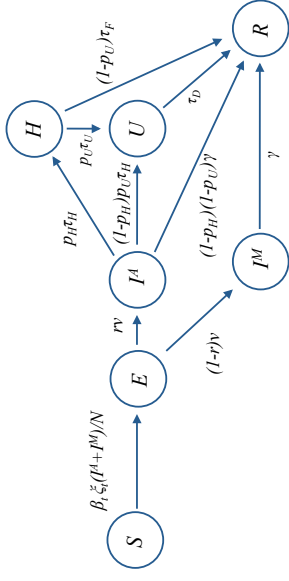


Figure S5: Model structure. Individuals start off susceptible to infection (S). Upon infection with Ebola they enter an incubation period (E), then at symptom onset they become infectious; these individuals either eventually become ascertained (I^A) or do not (I^M). Individuals who are ascertained initially seek health care in EHC/CCCs (or ETUs if these are full); if no beds are available, they remain infectious in the community until the infection is resolved (R) i.e. they have recovered, or are dead and buried. Patients in EHC/CCCs are transferred to ETUs once they have been tested for Ebola, which takes an average of 2 days. Patients remain in ETUs until the infection is resolved. We assume the latent period is 9.4 days, the average time from onset to EHC/CCC attendance is 4.6 days, and individuals who do not seek treatment are infectious for 11.3 days on average[1].

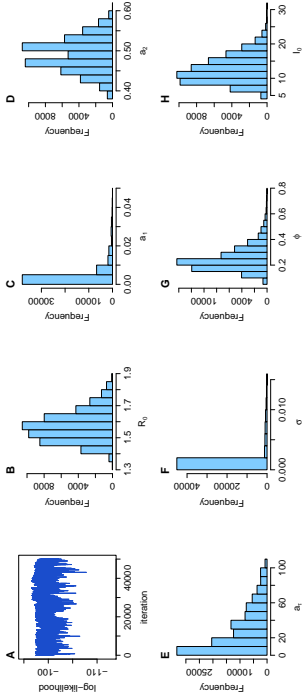


Figure S6: Estimated posterior parameter distributions for Bo. (A) MCMC trace plot of log-likelihood. (B) Basic reproduction number at the start of the outbreak in the district, $R_0 = \beta_0/\gamma$. (C) Slope of the time-varying transmission rate sigmoid, a_1 . (D) Final value of sigmoid, a_2 . (E) Midpoint of sigmoid, a_r . (F) Volatility of transmission noise, σ . (G) Reporting error, ϕ . (H) Initial number of infectious individuals, I_0 .

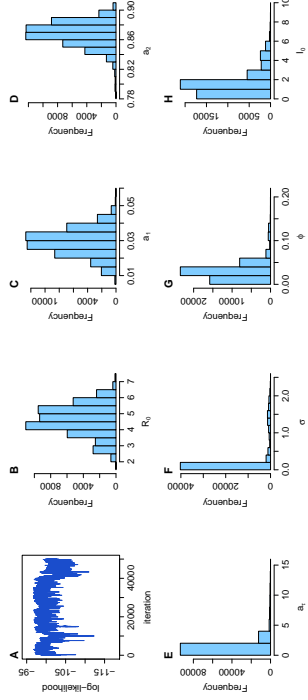


Figure S7: Estimated posterior parameter distributions for Bombali. (A) MCMC trace plot of log-likelihood. (B) Basic reproduction number at the start of the outbreak in the district, $R_0 = \beta_0/\gamma$. (C) Slope of the time-varying transmission rate sigmoid, a_1 . (D) Final value of sigmoid, a_2 . (E) Midpoint of sigmoid, a_r . (F) Volatility of transmission noise, σ . (G) Reporting error, ϕ . (H) Initial number of infectious individuals, I_0 .

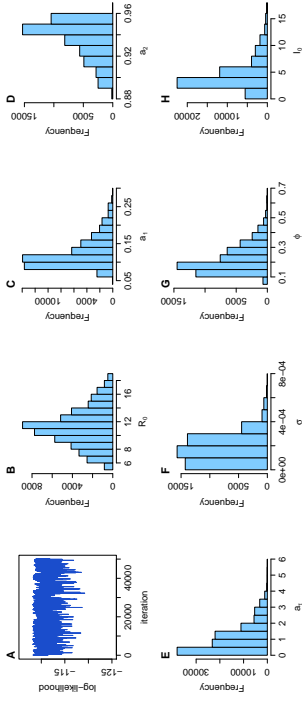


Figure S8: Estimated posterior parameter distributions for Kailahun. (A) MCMC trace plot of log-likelihood. (B) Basic reproduction number at the start of the outbreak in the district, $R_0 = \beta_0/\gamma$. (C) Slope of the time-varying transmission rate sigmoid, a_1 . (D) Final value of sigmoid, a_2 . (E) Midpoint of sigmoid, a_2 . (F) Volatility of transmission noise, σ . (G) Reporting error, ϕ . (H) Initial number of infectious individuals, I_0 .

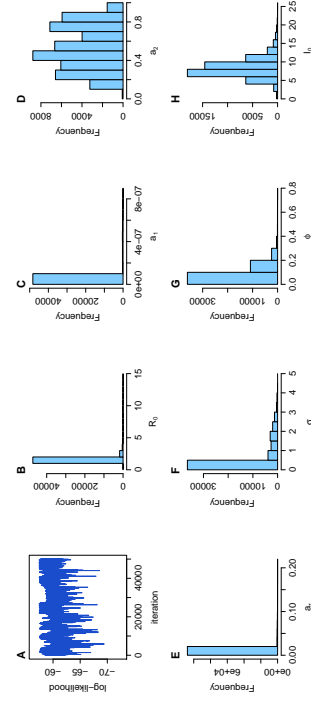


Figure S9: Estimated posterior parameter distributions for Kambia. (A) MCMC trace plot of log-likelihood. (B) Basic reproduction number at the start of the outbreak in the district, $R_0 = \beta_0/\gamma$. (C) Slope of the time-varying transmission rate sigmoid, a_1 . (D) Final value of sigmoid, a_2 . (E) Midpoint of sigmoid, a_2 . (F) Volatility of transmission noise, σ . (G) Reporting error, ϕ . (H) Initial number of infectious individuals, I_0 .

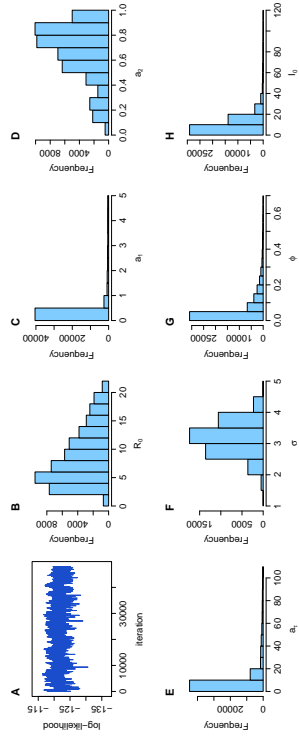


Figure S10: Estimated posterior parameter distributions for Kenema. (A) MCMC trace plot of log-likelihood. (B) Basic reproduction number at the start of the outbreak in the district, $R_0 = \beta_0/\gamma$. (C) Slope of the time-varying transmission rate sigmoid, a_1 . (D) Final value of sigmoid, a_2 . (E) Midpoint of sigmoid, a_τ . (F) Volatility of transmission noise, σ . (G) Reporting error, ϕ . (H) Initial number of infectious individuals, I_0 .

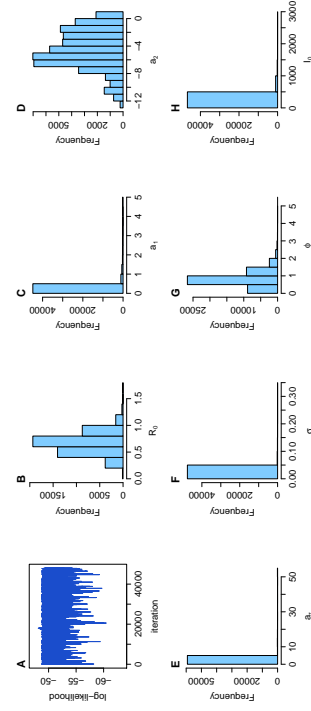


Figure S11: Estimated posterior parameter distributions for Koinadugu. (A) MCMC trace plot of log-likelihood. (B) Basic reproduction number at the start of the outbreak in the district, $R_0 = \beta_0/\gamma$. (C) Slope of the time-varying transmission rate sigmoid, a_1 . (D) Final value of sigmoid, a_2 . (E) Midpoint of sigmoid, a_τ . (F) Volatility of transmission noise, σ . (G) Reporting error, ϕ . (H) Initial number of infectious individuals, I_0 .

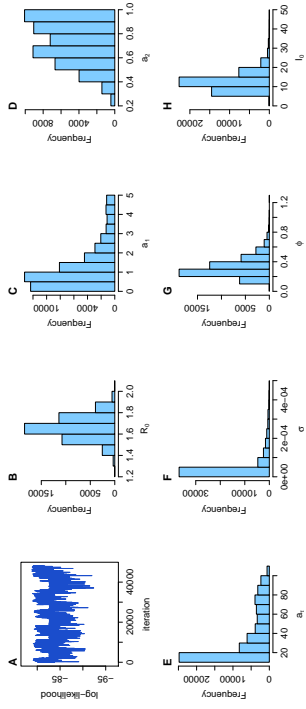


Figure S12: Estimated posterior parameter distributions for Kono. (A) MCMC trace plot of log-likelihood. (B) Basic reproduction number at the start of the outbreak in the district, $R_0 = \beta_0/\gamma$. (C) Slope of the time-varying transmission rate sigmoid, a_1 . (D) Final value of sigmoid, a_2 . (E) Midpoint of sigmoid, a_r . (F) Volatility of transmission noise, σ . (G) Reporting error, ϕ . (H) Initial number of infectious individuals, I_0 . The bimodal distribution of the log-likelihood is the result of the two peaks in epidemic time series; the model switches between these peaks when fitting the sigmoid, which leads to the broad posterior distribution for a_r .

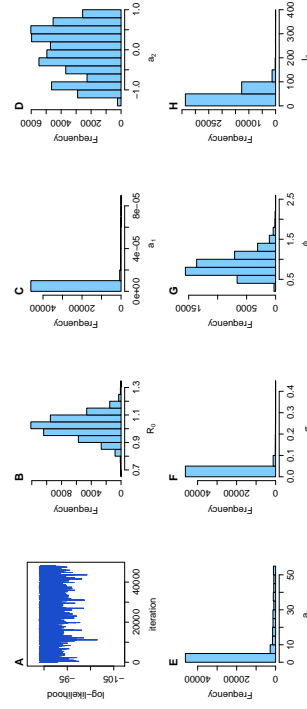


Figure S13: Estimated posterior parameter distributions for Moyamba. (A) MCMC trace plot of log-likelihood. (B) Basic reproduction number at the start of the outbreak in the district, $R_0 = \beta_0/\gamma$. (C) Slope of the time-varying transmission rate sigmoid, a_1 . (D) Final value of sigmoid, a_2 . (E) Midpoint of sigmoid, a_r . (F) Volatility of transmission noise, σ . (G) Reporting error, ϕ . (H) Initial number of infectious individuals, I_0 .

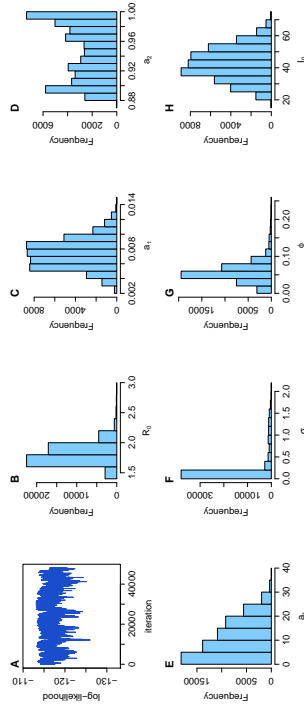


Figure S14: Estimated posterior parameter distributions for Port Loko. (A) MCMC trace plot of log-likelihood. (B) Basic reproduction number at the start of the outbreak in the district, $R_0 = \beta_0/\gamma$. (C) Slope of the time-varying transmission rate sigmoid, a_1 . (D) Final value of sigmoid, a_2 . (E) Midpoint of sigmoid, a_r . (F) Volatility of transmission noise, σ . (G) Reporting error, ϕ . (H) Initial number of infectious individuals, I_0 .

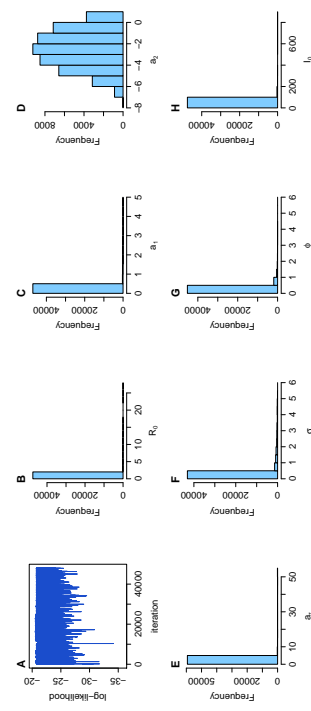


Figure S15: Estimated posterior parameter distributions for Pujehun. (A) MCMC trace plot of log-likelihood. (B) Basic reproduction number at the start of the outbreak in the district, $R_0 = \beta_0/\gamma$. (C) Slope of the time-varying transmission rate sigmoid, a_1 . (D) Final value of sigmoid, a_2 . (E) Midpoint of sigmoid, a_r . (F) Volatility of transmission noise, σ . (G) Reporting error, ϕ . (H) Initial number of infectious individuals, I_0 .

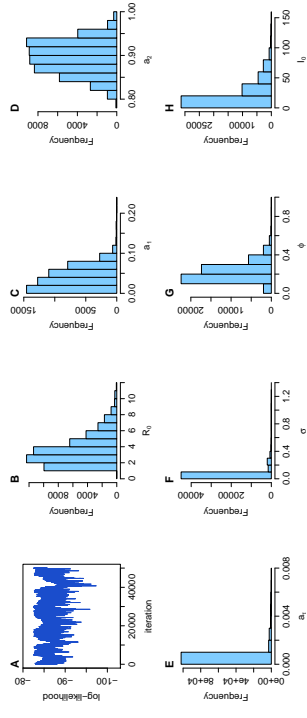


Figure S16: Estimated posterior parameter distributions for Tonkolili. (A) MCMC trace plot of log-likelihood. (B) Basic reproduction number at the start of the outbreak in the district, $R_0 = \beta_0/\gamma$. (C) Slope of the time-varying transmission rate sigmoid, a_1 . (D) Final value of sigmoid, a_2 . (E) Midpoint of sigmoid, a_{τ} . (F) Volatility of transmission noise, σ . (G) Reporting error, ϕ . (H) Initial number of infectious individuals, I_0 .

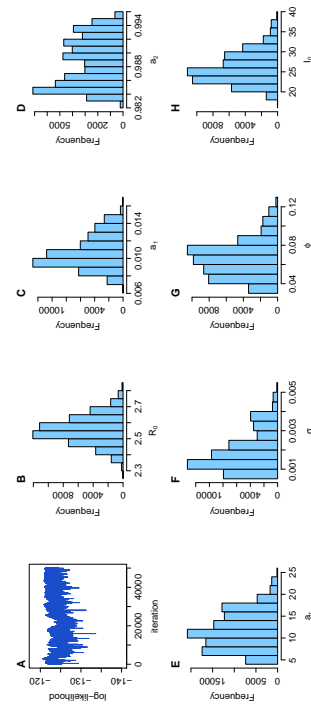


Figure S17: Estimated posterior parameter distributions for Western Area. (A) MCMC trace plot of log-likelihood. (B) Basic reproduction number at the start of the outbreak in the district, $R_0 = \beta_0/\gamma$. (C) Slope of the time-varying transmission rate sigmoid, a_1 . (D) Final value of sigmoid, a_2 . (E) Midpoint of sigmoid, a_{τ} . (F) Volatility of transmission noise, σ . (G) Reporting error, ϕ . (H) Initial number of infectious individuals, I_0 .

RESEARCH ARTICLE

Assessing the performance of real-time epidemic forecasts: A case study of Ebola in the Western Area region of Sierra Leone, 2014–15

Sebastian Funk^{1,2,*}, **Anton Camacho**^{1,2,3}, **Adam J. Kucharski**^{1,2}, **Rachel Lowe**^{1,2,4},
Rosalind M. Eggo^{1,2}, **W. John Edmunds**^{1,2}

1 Centre for the Mathematical Modelling of Infectious Diseases, London School of Hygiene & Tropical Medicine, London, United Kingdom, **2** Department of Infectious Disease Epidemiology, London School of Hygiene & Tropical Medicine, London, United Kingdom, **3** Epicentre, Paris, France, **4** Barcelona Institute for Global Health (ISGlobal), Barcelona, Spain

* sebastian.funk@lshtm.ac.uk



Abstract

OPEN ACCESS

Citation: Funk S, Camacho A, Kucharski AJ, Lowe R, Eggo RM, Edmunds JW (2019) Assessing the performance of real-time epidemic forecasts: A case study of Ebola in the Western Area region of Sierra Leone, 2014–15. PLoS Comput Biol 15(2): e106785. <https://doi.org/10.1371/journal.pcbi.106785>

Editor: Christian Althaus, University of Bern, SWITZERLAND

Received: April 25, 2018

Accepted: January 14, 2019

Published: February 11, 2019

Copyright: © 2019 Funk et al. This is an open access article distributed under the terms of the Creative Commons Attribution license, which permits unrestricted use, distribution, and reproduction in any medium, provided the original author and source are credited.

Data Availability Statement: All data and code are contained in an R package available at <https://doi.org/10.5281/zenodo.2547701>.

Funding: This work was funded by the Research for Health in Humanitarian Crises (R2HC) Programme, managed by Research for Humanitarian Assistance (Grant 13166). SF, AJK and AC were supported by fellowships from the UK Medical Research Council (SF: MR/K021680/1, AC: MR/J01482X/1, AJK: MR/K021524/1). SF was

Real-time forecasts based on mathematical models can inform critical decision-making during infectious disease outbreaks. Yet, epidemic forecasts are rarely evaluated during or after the event, and there is little guidance on the best metrics for assessment. Here, we propose an evaluation approach that disentangles different components of forecasting ability using metrics that separately assess the calibration, sharpness and bias of forecasts. This makes it possible to assess not just how close a forecast was to reality but also how well uncertainty has been quantified. We used this approach to analyse the performance of weekly forecasts we generated in real time for Western Area, Sierra Leone, during the 2013–16 Ebola epidemic in West Africa. We investigated a range of forecast model variants based on the model fits generated at the time with a semi-mechanistic model, and found that good probabilistic calibration was achievable at short time horizons of one or two weeks ahead but model predictions were increasingly unreliable at longer forecasting horizons. This suggests that forecasts may have been of good enough quality to inform decision making based on predictions a few weeks ahead of time but no longer, reflecting the high level of uncertainty in the processes driving the trajectory of the epidemic. Comparing forecasts based on the semi-mechanistic model to simpler null models showed that the best semi-mechanistic model variant performed better than the null models with respect to probabilistic calibration, and that this would have been identified from the earliest stages of the outbreak. As forecasts become a routine part of the toolkit in public health, standards for evaluation of performance will be important for assessing quality and improving credibility of mathematical models, and for elucidating difficulties and trade-offs when aiming to make the most useful and reliable forecasts.

supported by a Wellcome Trust Senior Research Fellowship in Basic Biomedical Science (210758/Z/18/Z). AJK was supported by a Sir Henry Dale Fellowship jointly funded by the Wellcome Trust and the Royal Society (206250/Z/17/Z). RL was supported by a Royal Society Dorothy Hodgkin fellowship. RME acknowledges funding from an HDR UK Innovation Fellowship (grant M/R/S003975/1). WJE and RME acknowledge funding from the Innovative Medicines Initiative 2 (IMI2) Joint Undertaking under grant agreement EB0VAC1 (grant 115854). The IMI2 is supported by the European Union Horizon 2020 Research and Innovation Programme and the European Federation of Pharmaceutical Industries and Associations. The funders had no role in study design, data collection and analysis, decision to publish, or preparation of the manuscript.

Competing interests: The authors have declared that no competing interests exist.

Author summary

During epidemics, reliable forecasts can help allocate resources effectively to combat the disease. Various types of mathematical models can be used to make such forecasts. In order to assess how good the forecasts are, they need to be compared to what really happened. Here, we describe different approaches to assessing how good forecasts were that we made with mathematical models during the 2013–16 West African Ebola epidemic, focusing on one particularly affected area of Sierra Leone. We found that, using the type of models we used, it was possible to reliably predict the epidemic for a maximum of one or two weeks ahead, but no longer. Comparing different versions of our model to simpler models, we further found that it would have been possible to determine the model that was most reliable at making forecasts from early on in the epidemic. This suggests that there is value in assessing forecasts, and that it should be possible to improve forecasts by checking how good they are during an ongoing epidemic.

Introduction

Forecasting the future trajectory of cases during an infectious disease outbreak can make an important contribution to public health and intervention planning. Infectious disease modelers are now routinely asked for predictions in real time during emerging outbreaks [1]. Forecasting targets can revolve around expected epidemic duration, size, or peak timing and incidence [2–5], geographical distribution of risk [6], or short-term trends in incidence [7, 8]. However, forecasts made during an outbreak are rarely investigated during or after the event for their accuracy, and only recently have forecasters begun to make results, code, models and data available for retrospective analysis.

The growing importance of infectious disease forecasts is epitomised by the growing number of so-called forecasting challenges. In these, researchers compete in making predictions for a given disease and a given time horizon. Such initiatives are difficult to set up during unexpected outbreaks, and are therefore usually conducted on diseases known to occur seasonally, such as dengue [7, 9, 10] and influenza [11]. The *Ebola Forecasting Challenge* was a notable exception, triggered by the 2013–16 West African Ebola epidemic and set up in June 2015. Since the epidemic had ended in most places at that time, the challenge was based on simulated data designed to mimic the behaviour of the true epidemic instead of real outbreak data. The main lessons learned were that 1) ensemble estimates outperformed all individual models, 2) more accurate data improved the accuracy of forecasts and 3) considering contextual information such as individual-level data and situation reports improved predictions [12].

In theory, infectious disease dynamics should be predictable within the timescale of a single outbreak [13]. In practice, however, providing accurate forecasts during emerging epidemics comes with particular challenges such as data quality issues and limited knowledge about the processes driving growth and decline in cases. In particular, uncertainty about human behavioural changes and public health interventions can preclude reliable long-term predictions [14, 15]. Yet, short-term forecasts with an horizon of a few generations of transmission (e.g., a few weeks in the case of Ebola), can yield important information on current and anticipated outbreak behaviour and, consequently, guide immediate decision making.

The most recent example of large-scale outbreak forecasting efforts was during the 2013–16 Ebola epidemic, which vastly exceeded the burden of all previous outbreaks with almost 30,000 reported cases resulting in over 10,000 deaths in the three most affected countries: Guinea, Liberia and Sierra Leone. During the epidemic, several research groups provided

forecasts or projections at different time points, either by generating scenarios believed plausible, or by fitting models to the available time series and projecting them forward to predict the future trajectory of the outbreak [116–126]. One forecast that gained particular attention during the epidemic was published in the summer of 2014, projecting that by early 2015 there might be 1.4 million cases [127]. This number was based on unmitigated growth in the absence of further intervention and proved a gross overestimate, yet it was later highlighted as a “call to arms” that served to trigger the international response that helped avoid the worst-case scenario [28]. While that was a particularly drastic prediction, most forecasts made during the epidemic were later found to have overestimated the expected number of cases, which provided a case for models that can generate sub-exponential growth trajectories [29, 30].

Traditionally, epidemic forecasts are assessed using aggregate metrics such as the mean absolute error (MAE) [12, 31, 32]. This, however, only assesses how close the most likely or average predicted outcome is to the true outcome. The ability to correctly forecast uncertainty, and to quantify confidence in a predicted event, is not assessed by such metrics. Appropriate quantification of uncertainty, especially of the likelihood and magnitude of worst case scenarios, is crucial in assessing potential control measures. Methods to assess probabilistic forecasts are now being used in other fields, but are not commonly applied in infectious disease epidemiology [33, 34].

We produced weekly sub-national real-time forecasts during the Ebola epidemic, starting on 28 November 2014. Plots of the forecasts were published on a dedicated web site and updated every time a new set of data were available [35]. They were generated using a model that has, in variations, been used to forecast bed demand during the epidemic in Sierra Leone [21] and the feasibility of vaccine trials later in the epidemic [36, 37]. During the epidemic, we provided sub-national forecasts for the three most affected countries (at the level of counties in Liberia, districts in Sierra Leone and prefectures in Guinea).

Here, we apply assessment metrics that elucidate different properties of forecasts, in particular their probabilistic calibration, sharpness and bias. Using these methods, we retrospectively assess the forecasts we generated for Western Area in Sierra Leone, an area that saw one of the greatest number of cases in the region and where our model informed bed capacity planning.

Materials and methods

Ethics statement

This study has been approved by the London School of Hygiene & Tropical Medicine Research Ethics Committee (reference number 8627).

Data sources

Numbers of suspected, probable and confirmed Ebola cases at sub-national levels were initially compiled from daily *Situation Reports* (or *SitReps*) provided in PDF format by Ministries of Health of the three affected countries during the epidemic [21]. Data were automatically extracted from tables included in the reports wherever possible and otherwise manually converted by hand to machine-readable format and aggregated into weeks. From 20 November 2014, the World Health Organization (WHO) provided tabulated data on the weekly number of confirmed and probable cases. These were compiled from the patient database, which was continuously cleaned and took into account reclassification of cases avoiding potential double-counting. However, the patient database was updated with substantial delay so that the number of reported cases would typically be underestimated in the weeks leading up to the date at which the forecast was made. Because of this, we used the *SitRep* data for the most recent

weeks until the latest week in which the WHO case counts either equalled or exceeded the SitRep counts. For all earlier times, the WHO data were used.

Transmission model

We used a semi-mechanistic stochastic model of Ebola transmission described previously [21, 38]. Briefly, the model was based on a Susceptible–Exposed–Infectious–Recovered (SEIR) model with fixed incubation period of 9.4 days [39], following an Erlang distribution with shape 2. The country-specific infectious period was determined by adding the average delay to hospitalisation to the average time from hospitalisation to death or discharge, weighted by the case-fatality rate. Cases were assumed to be reported with a stochastic time-varying delay. On any given day, this was given by a gamma distribution with mean equal to the country-specific average delay from onset to hospitalisation and standard deviation of 0.1 day. We allowed transmission to vary over time in order to capture behavioural changes in the community, public health interventions or other factors affecting transmission for which information was not available at the time. The time-varying transmission rate was modelled using a daily Gaussian random walk with fixed volatility (or standard deviation of the step size) which was estimated as part of the inference procedure (see below). We log-transformed the transmission rate to ensure it remained positive. The behaviour in time can be written as

$$d \log \beta_t = \sigma dW_t \quad (1)$$

where β_t is the time-varying transmission rate, W_t is the Wiener process and σ the volatility of the transmission rate. The basic reproduction number $R_{0,t}$ at any time was obtained by multiplying β_t with the average infectious period. In fitting the model to the time series of cases we extracted posterior predictive samples of trajectories, which we used to generate forecasts.

Model fitting

Each week, we fitted the model to the available case data leading up to the date of the forecast. Observations were assumed to follow a negative binomial distribution. Since the *ssm* software used to fit the model only implemented a discretised normal observation model, we used a normal approximation of the negative binomial for observations, potentially introducing a bias at small counts. Four parameters were estimated in the process: the initial basic reproduction number R_0 (uniform prior within (1, 5)), initial number of infectious people (uniform prior within (1, 400)), overdispersion of the (negative binomial) observation process (uniform prior within (0, 0.5)) and volatility of the time-varying transmission rate (uniform prior within (0, 0.5)). We confirmed from the posterior distributions of the parameters that these priors did not set any problematic bounds. Samples of the posterior distribution of parameters and state trajectories were extracted using particle Markov chain Monte Carlo [40] as implemented in the *ssm* library [41]. For each forecast, 50,000 samples were extracted and thinned to 5000.

Predictive model variants

We used the samples of the posterior distribution generated using the Monte Carlo sampler to produce predictive trajectories, using the final values of estimated state trajectories as initial values for the forecasts and simulating the model forward for up to 10 weeks. While all model fits were generated using the same model described above, we tested a range of different predictive model variants to assess the quality of ensuing predictions. We tested variants where trajectories were stochastic (with demographic stochasticity and a noisy reporting process), as well as ones where these sources of noise were removed for predictions. We further tested predictive model variants where the transmission rate continued to follow a random walk

(unbounded, on a log-scale), as well as ones where the transmission rate stayed fixed during the forecasting period. When the transmission rate remained fixed for prediction, we tested variants where we used the final value of the transmission rate and ones where this value was averaged over a number of weeks leading up to the final fitted point, to reduce the potential influence of the last time point, at which the transmission rate may not have been well identified. We tested variants where the predictive trajectory was based on the final values and start at the last time point, and ones where it started at the penultimate time point, which could, again, be expected to be better informed by the data. For each model and forecast horizon, we generated point-wise medians and credible intervals from the sample trajectories.

Null models

To assess the performance of the semi-mechanistic transmission model we compared it to three simpler null models: two representing the constituent parts of the semi-mechanistic model, and a non-mechanistic time series model. For the first null model, we used a *deterministic* model that only contained the mechanistic core of the semi-mechanistic model, that is a deterministic SEIR model with fixed transmission rate and parameters otherwise the same as in the model described before [21]:

$$\frac{dS}{dt} = -\frac{R_0 I_c + I_h}{N} S \quad (2)$$

$$\frac{dE_1}{dt} = -\frac{R_0 I_c + I_h}{N} S - 2vE_1 \quad (3)$$

$$\frac{dE_2}{dt} = 2vE_1 - 2vE_2 \quad (4)$$

$$\frac{dI_c}{dt} = 2vE_2 - \tau I_c \quad (5)$$

$$\frac{dI_h}{dt} = \tau I_c - \gamma I_h \quad (6)$$

$$\begin{aligned} \frac{dR}{dt} &= \gamma I_h \\ \frac{dA}{dt} &= \tau I_c \end{aligned} \quad (7) \quad (8)$$

$$Y_t \sim \text{NB}(A_t - A_{t-1}, \phi) \quad (9)$$

where Y_t are observations at times t , S is the number susceptible, E the number infected but not yet infectious (split into two compartments for Erlang-distributed permanence times with shape 2), I_c is the number infectious and not yet notified, I_h is the number infectious and notified, R is the number recovered or dead, A is an accumulator for incidence, R_0 is the basic reproduction number, $\Delta = 1/\tau + 1/\gamma$ is the mean time from onset to outcome, $1/\nu$ is the mean incubation period, $1/\tau + 1/\gamma$ is the mean duration of infectiousness, $1/\tau$ is the mean time from onset to hospitalisation, $1/\gamma$ the mean duration from notification to outcome and $\text{NB}(\mu, \phi)$ is a negative binomial distribution with mean μ and overdispersion ϕ . All these parameters were informed by individual patient observations [39] except the overdispersion in reporting ϕ , and

the basic reproduction number R_0 , which were inferred using Markov-chain Monte Carlo with the same priors as in the semi-mechanistic model.

For the second null model, we used an *unfocused* model where the weekly incidence Z itself was modelled using a stochastic volatility model (without drift), that is a daily Gaussian random walk, and forecasts generated assuming the weekly number of new cases was not going to change:

$$\mathrm{d}\log Z = \sigma \mathrm{d}W \quad (10)$$

$$Y_t \sim \mathrm{NB}(Z_t, \phi) \quad (11)$$

where Y are observations, σ is the intensity of the random walk and ϕ the overdispersion of reporting (both estimated using Markov-chain Monte Carlo) and $\mathrm{d}W$ is the Wiener process.

Lastly, we used a null model based on a non-mechanistic Bayesian autoregressive AR(1) time series model:

$$x_{t+1} \sim \mathcal{N}(\phi x_t, \sigma_x) \quad (12)$$

$$Y_t^* \sim \mathcal{N}(x_t, \sigma_y) \quad (13)$$

$$Y_t = \max(0, [Y_t^*]) \quad (14)$$

where ϕ , σ_x and σ_y were estimated using Markov-chain Monte Carlo, and $[\dots]$ indicates rounding to the nearest integer. An alternative model with Poisson distributed observations was discarded as it yielded poorer predictive performance.

The deterministic and unfocused models were implemented in *libbi* [42] via the *RBi* [43] and *RBi.helpers* [44] R packages [45]. The Bayesian autoregressive time series model was implemented using the *bsts* package [46].

Metrics

The paradigm for assessing probabilistic forecasts is that they should maximise the sharpness of predictive distributions subject to calibration [47]. We therefore first assessed model calibration at a given forecasting horizon, before assessing their sharpness and other properties.

Calibration or reliability [48] of forecasts is the ability of a model to correctly identify its own uncertainty in making predictions. In a model with perfect calibration, the observed data at each time point look as if they came from the predictive probability distribution at that time. Equivalently, one can inspect the probability integral transform of the predictive distribution at time t [49],

$$u_t = F_t(x_t) \quad (15)$$

where x_t is the observed data point at time $t \in t_1, \dots, t_n$, n being the number of forecasts, and F_t is the (continuous) predictive cumulative probability distribution at time t . If the true probability distribution of outcomes at time t is G_t , then the forecasts F_t are said to be *ideal* if $F_t = G_t$ at all times t . In that case, the probabilities u_t are distributed uniformly.

In the case of discrete outcomes such as the incidence counts that were forecast here, the PIT is no longer uniform even when forecasts are ideal. In that case a randomised PIT can be used instead:

$$u_t = P_t(k_t) + \nu(P_t(k_t) - P_t(k_t - 1)) \quad (16)$$

where k_t is the observed count, $P_t(x)$ is the predictive cumulative probability of observing

incidence k at time t , $P_t(-1) = 0$ by definition and v is standard uniform and independent of k . If P_t is the true cumulative probability distribution, then u_t is standard uniform [50]. To assess calibration, we applied the Anderson-Darling test of uniformity to the probabilities u_t . The resulting p-value was a reflection of how compatible the forecasts were with the null hypothesis of uniformity of the PIT, or of the data coming from the predictive probability distribution. We calculated the mean p-value of 10 samples from the randomised PIT and found the corresponding Monte-Carlo error to be negligible (maximum standard deviation: $s_p = 0.003$). We considered that there was no evidence to suggest a forecasting model was miscalibrated if the p-value found was greater than a threshold of $p \geq 0.1$, some evidence that it was miscalibrated if $0.01 < p < 0.1$, and good evidence that it was miscalibrated if $p \leq 0.01$. In this context it should be noted, though, that uniformity of the (randomised) PIT is a necessary but not sufficient condition of calibration [47]. The p-values calculated here merely quantify our ability to reject a hypothesis of good calibration, but cannot guarantee that a forecast is calibrated. Because of this, other indicators of forecast quality must be considered when choosing a model for forecasts.

All of the following metrics are evaluated at every single data point. In order to compare the forecast quality of models, they were averaged across the time series.

Sharpness is the ability of the model to generate predictions within a narrow range of possible outcomes. It is a data-independent measure, that is, it is purely a feature of the forecasts themselves. To evaluate sharpness at time t , we used the normalised median absolute deviation about the median (MADN) of y

$$S_t(P_t) = \frac{1}{0.675} \text{median}(|y - \text{median}(y)|) \quad (17)$$

where y is a variable with CDF P_t , and division by 0.675 ensures that if the predictive distribution is normal this yields a value equivalent to the standard deviation. The MAD (i.e., the MADN without the normalising factor) is related to the interquartile range (and in the limit of infinite sample size takes twice its value), a common measure of sharpness [33], but is more robust to outliers [51]. The sharpest model would focus all forecasts on one point and have $S = 0$, whereas a completely blurred forecast would have $S \rightarrow \infty$. Again, we used Monte-Carlo samples from P_t to estimate sharpness.

We further assessed the *bias* of forecasts to test whether a model systematically over- or underpredicted. We defined the forecast bias at time t as

$$B_t(P_t, x_t) = 1 - (P_t(x_t) + P_t(x_t - 1)) \quad (18)$$

The least biased model would have exactly half of predictive probability mass not concentrated on the data itself below the data at time t and $B_t = 0$, whereas a completely biased model would yield either all predictive probability mass above ($B_t = 1$) or below ($B_t = -1$) the data.

We further evaluated forecasts using two *proper scoring rules*, that is scores which are minimised if the predictive distribution is the same as the one generating the data. These scores combine the assessment of calibration and sharpness for comparison of overall forecasting skill. The *Ranked Probability Score* (RPS) [52, 53] for count data is defined as [50]

$$\text{RPS}(P_t, x_t) = \sum_{k=0}^{\infty} (P_t(k) - \mathbb{1}(k \geq x_t))^2. \quad (19)$$

It reduces to the mean absolute error (MAE) if the forecast is deterministic and can therefore be seen as its probabilistic generalisation for discrete forecasts. A convenient equivalent

formulation for predictions generated from Monte-Carlo samples is [47, 50]

$$\text{RPS}(P_r, X) = \mathbb{E}_{P_r} |X - X_r| - \frac{1}{2} \mathbb{E}_{P_r} |X - X'|, \quad (20)$$

where X and X' are independent realisations of a random variable with cumulative distribution P_r .

The *David-Sebastiani score* (DSS) only considers the first two moments of the predictive distribution and is defined as [50]

$$\text{DSS}(P_r, X_r) = \left(\frac{x_r - \mu_{P_r}}{\sigma_{P_r}} \right)^2 + 2 \log \sigma_{P_r} \quad (21)$$

where μ_{P_r} and σ_{P_r} are the mean and standard deviation of the predictive probability distribution, respectively, estimated here using Monte-Carlo samples.

For comparison, we also evaluated forecasts using the *absolute error* (AE) of the median forecast, that is

$$\text{AE}(P_r, X_r) = |\text{median}_{P_r}(X) - x_r| \quad (22)$$

where X is a random variable with cumulative distribution P_r .

All scoring metrics used are implemented in the R package accompanying the paper. The *gofest* package was used for the Anderson-Darling test [54] and the *scoringRules* package for the RPS and DSS [55].

Results

The semi-mechanistic model used to generate real-time forecasts during the epidemic was able to reproduce the trajectories up to the date of each forecast, following the data closely by means of the smoothly varying transmission rate (Fig 1). The overall behaviour of the reproduction number (ignoring depletion of susceptibles which did not play a role at the population level given the relatively small proportion of the population infected) was one of a near-monotonic decline, from a median estimate of 2.9 (interquartile range (IQR) 2.1–4, 90% credible interval (CI) 1.2–6.9) in the first fitted week (beginning 10 August, 2014) to a median estimate of 1.3 (IQR 0.9–1.9, 90% CI 0.4–3.7) in early November, 0.9 (IQR 0.6–1.3, 90% CI 0.2–2.2) in

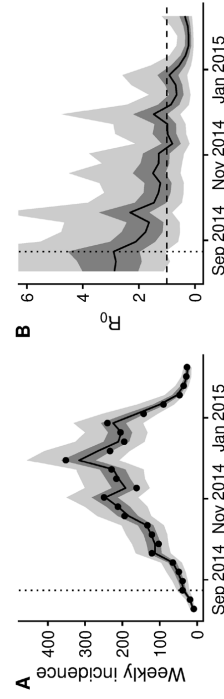


Fig 1. Final fit of the semi-mechanistic model to the Ebola outbreak in Western Area, Sierra Leone. (A) Final fit of the reported weekly incidence (black line and grey shading) to the data (black dots). (B) Corresponding dynamics of the reproduction number (ignoring depletion of susceptibles). Point-wise median state estimates are indicated by a solid line, interquartile ranges by dark shading, and 90% intervals by light shading. The threshold reproduction number ($R_0 = 1$), determining whether case numbers are expected to increase or decrease, is indicated by a dashed line. In both plots, a dotted vertical line indicates the date of the first forecast assessed in this manuscript (24 August 2014).

<https://doi.org/10.1371/journal.pcbi.1006785.g001>

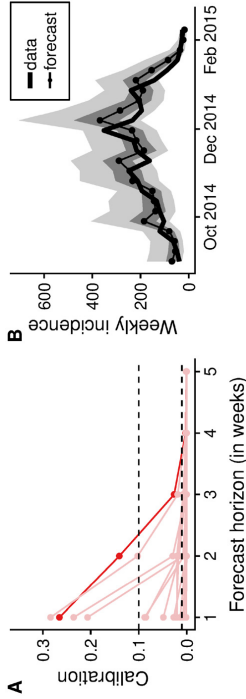


Fig 2. Calibration of forecasts from the semi-mechanistic model. (A) Calibration of predictive model variants (p -value of the Anderson-Darling test of uniformity) as a function of the forecast horizon. Shown in dark red is the best calibrated forecasting model variant (corresponding to the second row of Table 1). Other model variants are shown in light red. (B) Comparison of one-week forecasts of reported weekly incidence generated using the best semi-mechanistic model variant to the subsequently released data. The data are shown as a thick line, and forecasts as dots connected by a thin line. Dark shades of grey indicate the point-wise interquartile range, and lighter shades of grey the point-wise 90% credible interval.

<https://doi.org/10.1371/journal.pcbi.1006785.g002>

early December, 0.6 in early January (IQR 0.3–0.8, 90% CI 0.1–1.5) and 0.3 at the end of the epidemic in early February (IQR 0.2–0.4, 90% CI 0.1–0.9).

The epidemic lasted for a total of 27 weeks, with forecasts generated starting from week 3. For m -week ahead forecasts this yielded a sample size of $25 - m$ forecasts to assess calibration. Calibration of forecasts from the semi-mechanistic model were good for a maximum of one or two weeks, but deteriorated rapidly at longer forecasting horizons (Fig 2). The two semi-mechanistic forecast model variants with best calibration performance used deterministic dynamics starting at the last fitted data point (Table 1). Of these two, the forecast model that kept the

Table 1. Calibration of forecast model variants of the semi-mechanistic model. Calibration (p -value of the Anderson-Darling test of uniformity) of deterministic and stochastic predictive model variants starting either at the last data point or one week before, with varying (according to a Gaussian random walk) or fixed transmission rate either starting from the last value of the transmission rate or from an average over the last 2 or 3 weeks. The p -values highlighted in bold reflect predictive models with no evidence of miscalibration. The second row corresponds to the highlighted model variant in Fig 2A.

Predictive model variant	Stochasticity	Start	Transmission	Averaged	Forecast horizon (weeks)			
					1	2	3	4
deterministic	at last data point	varying	no	0.28	0.1	0.02	<0.01	<0.01
deterministic	at last data point	fixed	no	0.26	0.14	0.03	<0.01	<0.01
deterministic	at last data point	fixed	2 weeks	0.24	0.03	<0.01	<0.01	<0.01
deterministic	at last data point	fixed	3 weeks	0.21	<0.01	<0.01	<0.01	<0.01
deterministic	1 week before	varying	no	0.05	0.02	<0.01	<0.01	<0.01
deterministic	1 week before	fixed	no	0.09	0.02	<0.01	<0.01	<0.01
deterministic	1 week before	fixed	2 weeks	0.09	<0.01	<0.01	<0.01	<0.01
deterministic	1 week before	fixed	3 weeks	0.03	<0.01	<0.01	<0.01	<0.01
stochastic	at last data point	varying	no	0.02	0.02	<0.01	<0.01	<0.01
stochastic	at last data point	fixed	no	0.02	0.02	<0.01	<0.01	<0.01
stochastic	at last data point	fixed	2 weeks	0.01	<0.01	<0.01	<0.01	<0.01
stochastic	at last data point	fixed	3 weeks	<0.01	<0.01	<0.01	<0.01	<0.01
stochastic	1 week before	varying	no	<0.01	<0.01	<0.01	<0.01	<0.01
stochastic	1 week before	fixed	no	<0.01	<0.01	<0.01	<0.01	<0.01
stochastic	1 week before	fixed	2 weeks	<0.01	<0.01	<0.01	<0.01	<0.01
stochastic	1 week before	fixed	3 weeks	<0.01	<0.01	<0.01	<0.01	<0.01

<https://doi.org/10.1371/journal.pcbi.1006785.t001>

transmission rate constant from the value at the last data point performed slightly better across forecast horizons than one that continued to change the transmission rate following a random walk with volatility estimated from the time series. There was no evidence of miscalibration in both of the models with best calibration performance for two-week ahead forecasts, but increasing evidence of miscalibration for forecast horizons of three weeks or more. Calibration of all model variants was poor four weeks or more ahead, and all the stochastic model variants were miscalibrated for any forecast horizon, including the one we used to publish forecasts during the Ebola epidemic (stochastic, starting at the last data point, no averaging of the transmission rate, no projected volatility).

The calibration of the best semi-mechanistic forecast model variant (deterministic dynamics, transmission rate fixed and starting at the last data point) was better than that of any of the null models (Fig 3A and Table 2) for up to three weeks. While there was no evidence for miscalibration of the autoregressive null model for 1-week-ahead forecasts, there was good evidence of miscalibration for longer forecast horizons. There was some evidence of miscalibration of the unfocused null model, which assumes that the same number of cases will be reported in the weeks following the week during which the forecast was made, for 1 week ahead and good evidence of miscalibration beyond. Calibration of the deterministic null model was poor for all forecast horizons.

The semi-mechanistic and deterministic models showed a tendency to overestimate the predicted number of cases, while the autoregressive and null models tended to underestimate (Fig 3B and Table 2). This bias increased with longer forecast horizons in all cases. The best calibrated semi-mechanistic model variant progressed from a 12% bias at 1 week ahead to 20% (2 weeks), 30% (3 weeks), 40% (4 weeks) and 44% (5 weeks) overestimation. At the same time, this model showed rapidly decreasing sharpness as the forecast horizon increased (Fig 3C and Table 2). This is reflected in the proper scoring rules that combine calibration and sharpness, with smaller values indicating better forecasts (Fig 3D and 3E and and Table 2). At 1-week ahead, the mean RPS values of the autoregressive, unfocused and best semi-mechanistic

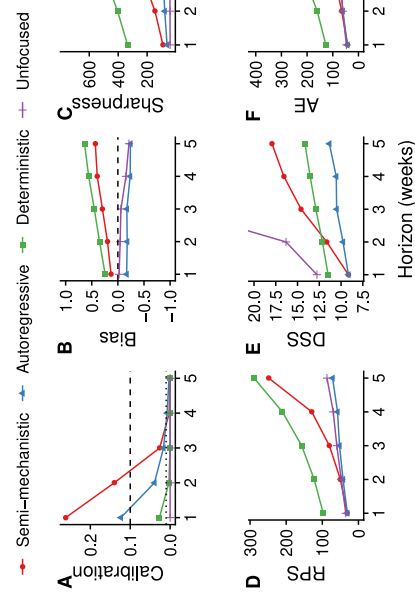


Fig 3. Forecasting metrics and scores of the best semi-mechanistic model variant compared to null models. Metrics shown are (A) calibration (p-value of Anderson-Darling test, greater values indicating better calibration, dashed lines at 0.1 and 0.01), (B) bias (less bias is better), (C) sharpness (MAD, sharper models having values closer to 0), (D) RPS (better values closer to 0), (E) DSS (better values closer to 0) and (F) AE (better values closer to 0), all as a function of the forecast horizon.

<https://doi.org/10.1371/journal.pcbi.1006785.g003>

Table 2. Forecasting metrics and scores of the best semi-mechanistic model variant compared to null models. The values shown are the same scores as in Fig 3, for forecasting horizons up to three weeks. The p-values for calibration highlighted in bold reflect predictive models with no evidence of miscalibration.

Model		Calibration	Sharpness	Bias	RPS	DSS	AE
1 week ahead							
Semi-mechanistic	0.26		91	0.13		31	9.2
Auto-regressive	0.1		61	-0.17	31	9.1	42
Deterministic	0.03		340	0.24	97	11	43
Unfocused	<0.01		41	-0.024	35	13	130
2 weeks ahead							
Semi-mechanistic	0.14		150	0.2	50	12	65
Auto-regressive	0.03		77	-0.18	43	9.9	60
Deterministic	<0.01		400	0.35	120	12	160
Unfocused	<0.01		42	-0.044	48	16	61
3 weeks ahead							
Semi-mechanistic	0.03		230	0.3	81	15	93
Auto-regressive	0.02		90	-0.17	53	11	73
Deterministic	<0.01		490	0.45	160	13	210
Unfocused	<0.01		44	-0.058	60	29	71

<https://doi.org/10.1371/journal.pcbi.1006785.t002>

forecasting models were all around 30. At increasing forecasting horizon, the RPS of the semi-mechanistic model grew faster than the RPS of the autoregressive and unfocused null models. The DSS of the semi-mechanistic model, on the other hand, was very similar to the one of the autoregressive and better than that of the other null models at a forecast horizon of 1 week, with the autoregressive again performing best at increasing forecast horizons.

Focusing purely on the median forecast (and thus ignoring both calibration and sharpness), the absolute error (AE, Fig 3F and Table 2) was lowest (42) for the best semi-mechanistic model variant at 1-week ahead forecasts, although similar to the autoregressive and unfocused null models. With increasing forecasting horizon, the absolute error increased at a faster rate for the semi-mechanistic model than for the autoregressive and unfocused null models.

We lastly studied the calibration behaviour of the models over time; that is, using the data and forecasts available up to different time points during the epidemic (Fig 4). This shows that from very early on, not much changed in the ranking of the different semi-mechanistic model variants. Comparing the best semi-mechanistic forecasting model to the null models, again, for almost the whole duration of the epidemic calibration of the semi-mechanistic model was best for forecasts 1 or 2 weeks ahead.

Discussion

Probabilistic forecasts aim to quantify the inherent uncertainty in predicting the future. In the context of infectious disease outbreaks, they allow the forecaster to go beyond merely providing the most likely future scenario and quantify how likely that scenario is to occur compared to other possible scenarios. While correctly quantifying uncertainty in predicted trajectories has not commonly been the focus in infectious disease forecasting, it can have enormous practical implications for public health planning. Especially during acute outbreaks, decisions are often made based on so-called “worst-case scenarios” and their likelihood of occurring. The ability to adequately assess the magnitude as well as the probability of such scenarios requires accuracy at the tails of the predictive distribution, in other words good calibration of the forecasts.

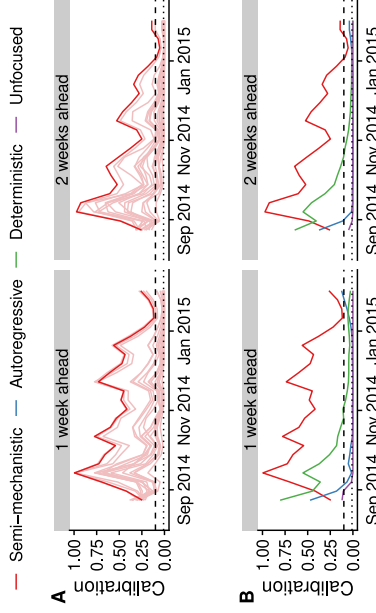


Fig 4. Calibration over time. Calibration scores of the forecast up to the time point shown on the x-axis. (A) Semi-mechanistic model variants, with the best model highlighted in dark red and other model variants are shown in light red. (B) Best semi-mechanistic model and null models. In both cases, 1-week (left) and 2-week (right) calibration (p-value of Anderson-Darling test) are shown.

<https://doi.org/10.1371/journal.pcbi.1006785.g004>

More generally, probabilistic forecasts need to be assessed using metrics that go beyond the simple difference between the central forecast and what really happened. Applying a suite of assessment methods to the forecasts we produced for Western Area, Sierra Leone, we found that probabilistic calibration of semi-mechanistic model variants varied, with the best ones showing good calibration for up to 2–3 weeks ahead, but performance deteriorated rapidly as the forecasting horizon increased. This reflects our lack of knowledge about the underlying processes shaping the epidemic at the time, from public health interventions by numerous national and international agencies to changes in individual and community behaviour. During the epidemic, we only published forecasts up to 3 weeks ahead, as longer forecasting horizons were not considered appropriate.

Our forecasts suffered from bias that worsened as the forecasting horizon expanded. Generally, the forecasts tended to overestimate the number of cases to be expected in the following weeks, as did most other forecasts generated during the outbreak [29]. This is in line with previous findings where our model was applied to predict simulated data of a hypothetical Ebola outbreak [38]. Log-transforming the transmission rate in order to ensure positivity skewed the underlying distribution and made very high values possible. Moreover, we did not model a trend in the transmission rate, whereas in reality transmission decreased over the course of the epidemic, probably due to a combination of factors ranging from better provision of isolation beds to increasing awareness of the outbreak and subsequent behavioural changes. While our model captured changes in the transmission rate in model fits, it did not forecast any trends such as the observed decrease over time. Capturing such trends in the attempt to identify underlying causes would be an important future improvement of real-time infectious disease models used for forecasting.

There are trade-offs between achieving good outcomes for the different forecast metrics we used. Deciding whether the best forecast is the best calibrated, the sharpest or the least biased, or some compromise between the three, is not a straightforward task. Our assessment of forecasts using separate metrics for probabilistic calibration, sharpness and bias highlights the underlying trade-offs. While the best calibrated semi-mechanistic model variant showed better calibration performance than the null models, this came at the expense of a decrease in the

sharpness of forecasts. Comparing the models using the RPS alone, the semi-mechanistic model of best calibration performance would not necessarily have been chosen. Following the paradigm of maximising sharpness subject to calibration, we therefore recommend to treat probabilistic calibration as a prerequisite to the use of forecasts, in line with what has recently been suggested for post-processing of forecasts [56]. Probabilistic calibration is essential for making meaningful probabilistic statements (such as the chances of seeing the number of cases exceed a set threshold in the upcoming weeks) that enable realistic assessments of resource demand, the possible future course of the epidemic including worst-case scenarios, as well as the potential impact of public health measures. Beyond the formal test for uniformity of the PIT applied here, alternative ways of assessing calibration can be used [47, 57]. Once a subset of models has been selected in an attempt to discard miscalibrated models, other criteria such as the RPS or DSS can be used to select the best model for forecasts, or to generate weights for ensemble forecasts combining several models. Such ensemble forecasts have become a standard in weather forecasting [58] and have more recently shown promise for infectious disease forecasts [12, 59, 60].

Other models may have performed better than the ones presented here. Because we did not have access to data that would have allowed us to assess the importance of different transmission routes (burials, hospitals and the community) we relied on a relatively simple, flexible model. The deterministic SEIR model we used as a null model performed poorly on all forecasting scores, and failed to capture the downturn of the epidemic in Western Area. On the other hand, a well-calibrated mechanistic model that accounts for all relevant dynamic factors and external influences could, in principle, have been used to predict the behaviour of the epidemic reliably and precisely. Yet, lack of detailed data on transmission routes and risk factors precluded the parameterisation of such a model and are likely to do so again in future epidemics in resource-poor settings. Future work in this area will need to determine the main sources of forecasting error, whether structural, observational or parametric, as well as strategies to reduce such errors [32].

In practice, there might be considerations beyond performance when choosing a model for forecasting. Our model combined a mechanistic core (the SEIR model) with non-mechanistic variable elements. By using a flexible non-parametric form of the time-varying transmission rate, the model provided a good fit to the case series despite high levels of uncertainty about the underlying process. Having a model with a mechanistic core came with the advantage of enabling the assessment of interventions just as with a traditional mechanistic model. For example, the impact of a vaccine could be modelled by moving individuals from the susceptible into the recovered compartment [36, 37]. At the same time, the model was flexible enough to visually fit a wide variety of time series, and this flexibility might mask underlying misspecifications. Whenever possible, the guiding principle in assessing real-time models and predictions for public health should be the quality of the recommended decisions based on the model results [61].

Epidemic forecasts played a prominent role in the response to and public awareness of the Ebola epidemic [28]. Forecasts have been used for vaccine trial planning against Zika virus [62] and will be called upon again to inform the response to the next emerging epidemic or pandemic threat. Recent advances in computational and statistical methods now make it possible to fit models in near-real time, as demonstrated by our weekly forecasts [35]. Such repeated forecasts are a prerequisite for the use of metrics that assess not only how close the predictions were to reality, but also how well uncertainty in the predictions has been quantified. An agreement on standards of forecast assessment is urgently needed in infectious disease epidemiology, and retrospective or even real-time assessment should become standard for epidemic forecasts to prove accuracy and improve end-user trust. The metrics we have used here or

variations thereof could become measures of forecasting performance that are routinely used to evaluate and improve forecasts during epidemics.

For forecast assessment to happen in practice, evaluation strategies must be planned before the forecasts are generated. In order for such evaluation to be performed retrospectively, all forecasts as well as the data, code and models they were based on should be made public at the time, or at least preserved and decisions recorded for later analysis. We published weekly updated aggregate graphs and numbers during the Ebola epidemic, yet for full transparency it would have been preferable to allow individuals to download raw forecast data for further analysis.

If forecasts are not only produced but also evaluated in real time, this can give valuable insights into strengths, limitations, and reasonable time horizons. In our case, by tracking the performance of our forecasts, we would have noticed the poor calibration of the model variant chosen for the forecasts presented to the public, and instead selected better calibrated variants. At the same time, we did not store the predictive distribution samples for any area apart from Western Area in order to better use available storage space, and because we did not deem such storage valuable at the time. This has precluded a broader investigation of the performance of our forecasts.

Research into modelling and forecasting methodology and predictive performance at times during which there is no public health emergency should be part of pandemic preparedness activities. To facilitate this, outbreak data must be made available openly and rapidly. Where available, combination of multiple sources, such as epidemiological and genetic data, could increase predictive power. It is only on the basis of systematic and careful assessment of forecast performance during and after the event that predictive ability of computational models can be improved and lessons learned to maximise their utility in future epidemics.

Author Contributions

Formal analysis: Sebastian Funk, Anton Camacho.

Methodology: Sebastian Funk, Anton Camacho, Adam J. Kucharski, Rachel Lowe, Rosalind M. Eggo, W. John Edmunds.

Writing – original draft: Sebastian Funk.

Writing – review & editing: Sebastian Funk, Anton Camacho, Adam J. Kucharski, Rachel Lowe, Rosalind M. Eggo, W. John Edmunds.

References

- Heesterbeek H, Anderson RM, Andreasen V, Bansal S, Angelis DD, Dye C, et al. Modeling Infectious Disease Dynamics in the Complex Landscape of Global Health. *Science*. 2015; 347(6227):aaa4339–aaa4339. <https://doi.org/10.1126/science.aaa4339> PMID: 25766240
- Goldstein E, Cobey S, Takahashi S, Miller JC, Lipsitch M. Predicting the epidemic sizes of influenza A/H1N1, A/H3N2, and B: a statistical method. *PLoS Med*. 2011; 8(7):e1001051. <https://doi.org/10.1371/journal.pmed.1001051> PMID: 21750666
- Nsoesie E, Marathe M, Brownstein J. Forecasting peaks of seasonal influenza epidemics. *PLoS currents*. 2013; 5. <https://doi.org/10.1371/currents.outbreaks.bb16879a23137022ea79a8c508bb03bc> PMID: 23873050
- Yang W, Cowling BJ, Lau EH, Shaman J. Forecasting influenza epidemics in Hong Kong. *PLoS Comput Biol*. 2015; 11(7):e1004383. <https://doi.org/10.1371/journal.pcbi.1004383> PMID: 26226185
- Dawson PM, Werkman M, Brooks-Pollock E, Tilesey MJ. Epidemic predictions in an imperfect world: modelling disease spread with partial data. *Proc R Soc B*. 2015; 282(1808): 20150205. <https://doi.org/10.1098/rspb.2015.0205> PMID: 25948687

6. Lowe R, Barcellos C, Coelho CA, Bailey TC, Coelho GE, Graham R, et al. Dengue outlook for the World Cup in Brazil: an early warning model framework driven by real-time seasonal climate forecasts. *The Lancet Infectious Diseases*. 2014; 14(7):619–626. [https://doi.org/10.1016/S1473-3099\(14\)70781-9](https://doi.org/10.1016/S1473-3099(14)70781-9) PMID: 24841859
7. Johansson MA, Reich NG, Hota A, Brownstein JS, Santillana M. Evaluating the performance of infectious disease forecasts: A comparison of climate-driven and seasonal dengue forecasts for Mexico. *Sci Rep*. 2016; 6:33707. <https://doi.org/10.1038/srep33707> PMID: 27665707
8. Liu F, Porco TC, Amza A, Kadri B, Nassirou B, West SK, et al. Short-term forecasting of the prevalence of trachoma: expert opinion, statistical regression, versus transmission models. *PLoS Neglected Tropical Diseases*. 2015; 9(8):e0200400. <https://doi.org/10.1371/journal.pntd.0004000> PMID: 26502380
9. National Oceanic and Atmospheric Administration. Dengue Forecasting. 2017. Available from: <http://dengueforecasting.noaa.gov/>.
10. Centres for Disease Control and Prevention. Epidemic Prediction Initiative; 2017. Available from: <https://predict.phiresearchlab.org/legacy/dengue/index.html>.
11. Biggerstaff M, Alper D, Dredze M, Fox S, Fung JCH, Hickmann KS, et al. Results from the centers for disease control and prevention's predict the 2013–2014 influenza A Season Challenge. *BMC Infect Dis*. 2016; 16(1):357. <https://doi.org/10.1186/s12879-016-1669-x>
12. Viboud C, Sun K, Gaffey R, Ajelli M, Fumanelli L, Merler S, et al. The RAPIDD ebola forecasting challenge: Synthesis and lessons learnt. *Epidemics*. 2018; 22:13–21. <https://doi.org/10.1016/j.epidem.2017.08.002> PMID: 28938414
13. Scarpino SV, Petri G. On the predictability of infectious disease outbreaks. [arXiv:1703.07317v4](https://arxiv.org/abs/1703.07317v4).
14. Moran KR, Fairchild G, Generous N, Hickmann K, Osthus D, Pridhorsky R, et al. Epidemic forecasting is messier than weather forecasting: The role of human behavior and internet data streams in epidemic forecast. *J Infect Dis*. 2016; 214(suppl_4):S404–S408. <https://doi.org/10.1093/infdis/jiw375> PMID: 28830111
15. Funk S, Ciglenecki I, Tiffany A, Gignoux E, Camacho A, Eggo RM, et al. The impact of control strategies and behavioural changes on the elimination of Ebola from Lofa County, Liberia. *Phil Trans Roy Soc B*. 2017; 372:20160302. <https://doi.org/10.1098/rstb.2016.0302>
16. Fisman D, Khoo E, Tuite A. Early epidemic dynamics of the west african 2014 ebola outbreak: estimates derived with a simple two-parameter model. *PLoS Curr Outbreaks*. 2014. <https://doi.org/10.1371/currents.outbreaks.89ec0cd7783f36958096ebbae97348d571>
17. Lewnard JA, Ndeffo Mbah ML, Alfarro-Murillo JA, Aliche FL, Bawo L, Nyenswah TG, et al. Dynamics and control of Ebola virus transmission in Monserreao, Liberia: a mathematical modelling analysis. *Lancet Infect Dis*. 2014; 14(12):1189–1195. [https://doi.org/10.1016/S1473-3099\(14\)70995-8](https://doi.org/10.1016/S1473-3099(14)70995-8) PMID: 25455986
18. Nishiura H, Chowell G. Early transmission dynamics of Ebola virus disease (EVD), West Africa, March to August 2014. *Euro Surveill*. 2014; 19:20894. <https://doi.org/10.2807/1560-7917.EU2014.19.36.20894> PMID: 252232919
19. Rivers CM, Lofgren ET, Marathe M, Eubank S, Lewis BL. Modeling the impact of interventions on an epidemic of Ebola in Sierra Leone and Liberia. *PLoS Curr Outbreaks*. 2014. <https://doi.org/10.1371/currents.outbreaks.4d41fe56fc05e9df30bddce323c56d084c>
20. Towers S, Patterson-Lomba O, Castillo-O-Chavez C. Temporal variations in the effective reproduction number of the 2014 West Africa Ebola outbreak. *PLoS Curr Outbreaks*. 2014. <https://doi.org/10.1371/currents.outbreaks.9edc4294ec4ec1fadad2831772b160c908>
21. Camacho A, Kucharski A, Akh-Sawary Y, White MA, Fiasche S, Baguelin M, et al. Temporal Changes in Ebola Transmission in Sierra Leone and Implications for Control Requirements: a Real-Time Modelling Study. *PLoS Curr Outbreaks*. 2015. <https://doi.org/10.1371/currents.outbreaks.406aeef5eeb33ec0051593e30836b05235ed2>
22. Dong F, Xu D, Wang Z, Dong W. Evaluation of ebola spreading in west africa and decision of optimal medicine delivery strategies based on mathematical models. *Infect Genet Evol*. 2015; 36:35–40. <https://doi.org/10.1016/j.meegid.2015.09.003> PMID: 263443852
23. Drake JM, Kaul RB, Alexander LW, O'Regan SM, Kramer AM, Pulliam JT, et al. Ebola cases and health system demand in Liberia. *PLoS Biol*. 2015; 13(1):e1002056. <https://doi.org/10.1371/journal.pbio.1002056> PMID: 25565384
24. Merler S, Ajelli M, Fumanelli L, Gomes MFC, y Pontón AP, Rossi L, et al. Spatiotemporal spread of the 2014 outbreak of Ebola virus disease in Liberia and the effectiveness of non-pharmaceutical interventions: a computational modelling analysis. *Lancet Infect Dis*. 2015; 15(2):204–211. [https://doi.org/10.1016/S1473-3099\(14\)71074-6](https://doi.org/10.1016/S1473-3099(14)71074-6) PMID: 25755618
25. Siattas C, Anastassopoulou C, Russo L, Grigoras C, Mylonakis E. Modeling the 2014 ebola virus epidemic—agent-based simulations, temporal analysis and future predictions for libera and

- sierra leone. PLOS Curr Outbreaks. 2015; <https://doi.org/10.1371/currents.outbreaks.8d5984114855fc4256639e1a18cd6c9>
26. White RA, MacDonald E, De Blasio BF, Nygård IK, Vold L, Røttingen JA. Projected treatment capacity needs in Sierra Leone. PLOS Curr Outbreaks. 2015.
27. Meitzer Ml, Atkins CY, Santibanez S, Knust B, Petersen BW, Ervin ED, et al. Estimating the future number of cases in the Ebola epidemic—Liberia and Sierra Leone. 2014–2015. MMWR Surveill Summ. 2014; 63 Suppl 3:1–14.
28. Frieden TR, Damon IK. Ebola in West Africa—CDC's role in epidemic detection, control, and prevention. Emerg Infect Dis. 2015; 21(11):1897. <https://doi.org/10.3201/eid2111.150949> PMID: 2644940
29. Chretien JP, Riley S, George DB. Mathematical modeling of the West Africa Ebola epidemic. eLife. 2015; 4:e09186. <https://doi.org/10.7554/elife.09186> PMID: 26646185
30. Chowell G, Viboud C, Simonsen L, Meier S, Vesprignani A. Perspectives on model forecasts of the 2014–2015 Ebola epidemic in West Africa: lessons and the way forward. BMC Med. 2017; 15(1):42. <https://doi.org/10.1186/s12916-017-0611-y> PMID: 28245814
31. Chowell G. Fitting dynamic models to epidemic outbreaks with quantified uncertainty: A primer for parameter uncertainty, identifiability, and forecasts. Infectious Disease Modelling. 2017; 2(3):375–398. <https://doi.org/10.1016/j.idm.2017.06.001> PMID: 29250607
32. Pei S, Shaman J. Counteracting structural errors in ensemble forecast of influenza outbreaks. Nature Communications. 2017; 8(1). <https://doi.org/10.1038/s41467-017-01033-1>
33. Gneiting T, Katzfuss M. Probabilistic Forecasting. Annu Rev Stat Appl. 2014; 1(1):125–151. <https://doi.org/10.1146/annurev-statistics-062713-085631>
34. Held L, Meyer S, Bracher J. Probabilistic forecasting in infectious disease epidemiology: the 13th Armistage lecture. Stat Med. 2017; 36(22):3443–3460. <https://doi.org/10.1002/sim.7363> PMID: 2866694
35. Cente for the Mathematical Modelling of Infectious Diseases. Visualisation and projections of the Ebola outbreak in West Africa; 2015. Available from: <http://mrcmcm.github.io/ebola/>.
36. Camacho A, Eggo RM, Funk S, Watson CH, Kucharski AJ, Edmunds WJ. Estimating the probability of demonstrating vaccine efficacy in the declining Ebola epidemic: a Bayesian modelling approach. BMJ Open. 2015; 5(12):e009346. <https://doi.org/10.1136/bmjopen-2015-009346> PMID: 26671958
37. Camacho A, Eggo R, Goeyvaerts N, Vandebosch A, Mogg R, Funk S, et al. Real-time dynamic modeling for the design of a cluster-randomized phase 3 Ebola vaccine trial in Sierra Leone. Vaccine. 2017;in press. <https://doi.org/10.1016/j.vaccine.2016.12.019>
38. Funk S, Camacho A, Kucharski AJ, Eggo RM, Edmunds WJ. Real-time forecasting of infectious disease dynamics with a stochastic semi-mechanistic model. Epidemics. 2018; 22:56–61. <https://doi.org/10.1016/j.epidem.2016.11.003> PMID: 28038870
39. WHO Ebola Response Team. Ebola Virus Disease in West Africa—The First 9 Months of the Epidemic and Forward Projections. N Engl J Med. 2014.
40. Andrieu C, Doucet A, Holenstein R. Particle Markov chain Monte Carlo methods. J R Stat Soc B. 2010; 72, pt. 3:289–342. <https://doi.org/10.1111/j.1467-9868.2009.00736.x>
41. Dureau J, Ballesteros S, Bogich T. SSM: Inference for time series analysis with State Space Models. arXiv. 2013; 1307:5626.
42. Murray L. Bayesian State-Space Modelling on High-Performance Hardware Using LibBi. Journal of Statistical Software, Articles. 2015; 67(10):1–36.
43. Jacob PE, Funk S, RBi: Rinterface to LibBi; 2019. Available from: <https://github.com/libbi/RBi>.
44. Funk S, iibi.helpers: iibi helper functions; 2019. Available from: <https://github.com/sbfink/RBi.helpers>.
45. R Core Team. R: A Language and Environment for Statistical Computing; 2018. Available from: <https://www.R-project.org/>.
46. Scott SL. bsts: Bayesian Structural Time Series; 2018. Available from: <https://CRAN.R-project.org/package=bsts>.
47. Gneiting T, Balabdaoui F, Raftery AE. Probabilistic forecasts: calibration and sharpness. J R Stat Soc B. 2007; 69(2):243–268. <https://doi.org/10.1111/j.1467-9868.2007.00587.x>
48. Friederichs P, Thorarinsdottir TL. Forecast verification for extreme value distributions with an application to probabilistic peak wind prediction. Environmetrics. 2012; 23(7):579–594. <https://doi.org/10.1002/env.2176>
49. David AP. Present Position and Potential Developments: Some Personal Views. Statistical Theory: The Prequential Approach. J R Stat Soc A. 1984; 147(2):278. <https://doi.org/10.2307/2981663>
50. Czado C, Gneiting T, Held L. Predictive model assessment for count data. Biometries. 2009; 65(4):1254–1261. <https://doi.org/10.1111/j.1541-0420.2009.01191.x> PMID: 19432783

51. Maronna RA, Martin RD, Yohai VJ, Salibián-Barrera M. Robust Statistics: Theory and Methods (with R). Wiley Series in Probability and Statistics. Wiley; 2018.
52. Epstein ES. A scoring system for probability forecasts of ranked categories. *J Appl Meteorol*. 1969; 8(6):985–987. [https://doi.org/10.1175/1520-0450\(1969\)008%3C985:ASSEPF%3E2.0.CO;2](https://doi.org/10.1175/1520-0450(1969)008%3C985:ASSEPF%3E2.0.CO;2)
53. Murphy AH. On the “ranked probability score”. *J Appl Meteorol*. 1969; 8(6):988–989. [https://doi.org/10.1175/1520-0450\(1969\)008%3C988:OTPS%3E2.0.CO;2](https://doi.org/10.1175/1520-0450(1969)008%3C988:OTPS%3E2.0.CO;2)
54. Faraway J, Marsaglia G, Marsaglia J, Baddeley A. goftest: Classical Goodness-of-Fit Tests for Univariate Distributions. 2017. Available from: <https://CRAN.R-project.org/package=goftest>.
55. Jordan A, Krige F, Lerch S. Evaluating probabilistic forecasts with scoringRules. *arXiv*; 1709.04743v2.
56. Wilks DS. Enforcing calibration in ensemble postprocessing. *Q J Roy Meteor Soc*. 2018; 144(710):76–84. <https://doi.org/10.1002/qj.3185>
57. Held L, Rueßbach K, Bahabodouzi F. A Score Regression Approach to Assess Calibration of Continuous Probabilistic Predictions. *Biometrics*. 2010; 66(4):1295–1305. <https://doi.org/10.1111/j.1541-0420.2010.01406.x> PMID: 20353460
58. Gneiting T, Raftery AE. Weather forecasting with ensemble methods. *Science*. 2005; 310(5746):248–249. <https://doi.org/10.1126/science.1115255> PMID: 16224011
59. Yamana TK, Kandula S, Shaman J. Superensemble forecasts of dengue outbreaks. *J R Soc Interface*. 2016; 13(123):20160410. <https://doi.org/10.1098/rsif.2016.0410> PMID: 27733698
60. Yamana TK, Kandula S, Shaman J. Individual versus superensemble forecasts of seasonal influenza outbreaks in the United States. *PLOS Comput Biol*. 2017; 13(11):e1005601. <https://doi.org/10.1371/journal.pcbi.1005601> PMID: 29107987
61. Probert WJM, Jewell CP, Werkhoven M, Fonnesbeck CJ, Goto Y, Runge MC, et al. Real-time decision-making during emergency disease outbreaks. *PLOS Comput Biology*. 2018; 14(7):e1006202. <https://doi.org/10.1371/journal.pcbi.1006202>
62. World Health Organization. Efficacy trials of ZIKV Vaccines: endpoints, trial design, site selection. WHO Workshop Meeting Report; 2017.